Available online at www.sciencedirect.com
SCIENCE DIRECT®
Biochemical and Biophysical Research Communications 315 (2004) 802–807
BBRC
www.elsevier.com/locate/ybbrc

Anterograde and retrograde intracellular trafficking of fluorescent cellular prion protein

Naomi S. Hachiya, Kota Watanabe, Makiko Yamada, Yuji Sakasegawa, and Kiyotoshi Kaneko*

Department of Cortical Function Disorders, National Institute of Neuroscience (NIN), National Center of Neurology and Psychiatry (NCNP), and Core Research for Evolutional Science and Technology (CREST), Japan Science and Technology Agency, Tokyo 187-8502, Japan

Received 22 January 2004

Abstract

In order to investigate the microtubule-associated intracellular trafficking of the NH2-terminal cellular prion protein (PrP^C) fragment [Biochem. Biophys. Res. Commun. 313 (2004) 818], we performed a real-time imaging of fluorescent PrP^C (GFP-PrP^C) in living cells. Such GFP-PrP^C exhibited an anterograde movement towards the direction of plasma membranes at a speed of 140–180 nm/s, and a retrograde movement inwardly at a speed of 1.0–1.2 μm/s. The anterograde and retrograde movements of GFP-PrP^C were blocked by a kinesin family inhibitor (AMP-PNP) and a dynein family inhibitor (vanadate), respectively. Furthermore, anti-kinesin antibody (α-kinesin) blocked its anterograde motility, whereas anti-dynein antibody (α-dynein) blocked its retrograde motility. These data suggested the kinesin family-driven anterograde and the dynein-driven retrograde movements of GFP-PrP^C. Mapping of the interacting domains of PrP^C identified amino acid residues indispensable for interactions with kinesin family: NH2-terminal mouse (Mo) residues 53–91 and dynein: NH2-terminal Mo residues 23–33, respectively. Our findings argue that the discrete N-terminal amino acid residues are indispensable for the anterograde and retrograde intracellular movements of PrP^C.

Keywords: Cellular prion protein; Green fluorescent protein; Microtubules; Kinesin family; Dynein

The posttranslational conformational change of the cellular isoform of prion protein (PrP^C) into the scrapie isoform of prion protein (PrP^{Sc}) is the fundamental process underlying the pathogenesis of the prion disease [2,3]. An initial degradation of PrP^C involves cleavage of the NH2-terminal fragment to produce a COOH-terminal 17-kDa polypeptide which was found in a Triton X-100 insoluble fraction [4], of which the cleavage site was mapped at the amino acid residues between the 3F4 (amino acids 108/111 in mouse (Mo) PrP) and the 13A5 (amino acids 138 in Mo PrP) epitopes [4–6]. Several groups reported that NH2-terminal fragment of the PrP functions as a putative targeting element [7,8] and is essential for both transport to the plasma membrane and modulation of endocytosis [9]. GFP-tagged version of PrP^C was found to be properly anchored at the cell surface and its distribution pattern was similar to that of the endogenous PrP^C, with labelling at the plasma membrane and in an intracellular perinuclear compartment [10–14].

We previously demonstrated the microtubule-associated intracellular localization of the NH2-terminal fluorescent PrP^C fragment [1] in Mo neuroblastoma neuro2a (N2a), known to be infectable with PrP^{Sc} [15] and HpL3-4 cells, a hippocampal cell line established from *prnp* gene-ablated mice [16], by utilizing double-labelled PrP^C. At a steady state level, we detected NH_2-terminally fluorescent-tagged PrP^C predominantly in the intracellular compartments, COOH-terminally fluorescent-tagged PrP^C mostly at the cell surface membranes overlapping with lipid rafts, and PrP^C in full length with the merged color in Golgi compartments. The NH_2-terminal PrP^C fragment, which may not reflect the distribution to any single specific organelle, congregated in the cytosol after the treatment with a microtubule

* Corresponding author. Fax: +81-42-346-1748.
E-mail address: kaneko@ncnp.go.jp (K. Kaneko).

0006-291X/$ - see front matter © 2004 Elsevier Inc. All rights reserved.
doi:10.1016/j.bbrc.2004.01.126

depolymerizer (nocodazole). Such microtubule-associated intracellular localization required at least the 1–91 amino acid residues of the NH2-terminal PrP^C fragment.

With this background, we performed a follow-up study of intracellular GFP-PrP^C by a real-time imaging, which demonstrated the anterograde and retrograde intracellular movements of the NH_2-terminal PrP^C fragment in N2a and HpL3-4 cells.

Materials and methods

Construction of GFP-PrP and the deletion mutants. GFP-PrP constructs were made as previously described [1], and the resulted plasmid was designated pSPOX-MHM2PrP::GFP. The series of deletion mutants were amplified by PCR from the pSPOX-MHM2PrP::GFP [1] using 5′-GCA ACC GTT ACC CAC CTC AGG GGG GTA CCC ATA ATC AGT GGA ACA AGC CC-3′ as the forward primer and the following backward primers: 5′-CTG AGG TGG GTA ACG GTT GCC TCC AGG GCT-3′ (for amino acid residues Δ53–91 in Mo PrP), 5′-CTG ATG TCG GCC TCT GCA AAG GTA TGG TGA GC-3′ and 5′-TTT GCA GAG GCC GAC ATC AGT CCA CAT AGT-3′ (Δ23–33), digested with *Bam*HI and *Xho*I, and replaced with the *BamHI–XhoI* fragment of pSPOX-MHM2PrP::GFP [17]. The resulted plasmids were verified by direct DNA sequencing.

Antibodies and drugs. Anti-kinesin and anti-dynein antibodies were purchased from Santa Cruz Biotechnology, and anti-γ-tubulin antibody was purchased from Sigma. Vanadate and AMP-PNP were purchased from CHEMICON and Sigma, respectively. Nocodazole was purchased from Sigma.

Cell cultures, DNA transfection, and drug treatments. Mo neuroblastoma neuro2a (N2a) cells known to be infectable with PrP^{Sc} [15] were obtained from American Tissue Culture Collection. A hippocampal cell line established from *prnp* gene-ablated mice (HpL3-4) was kindly provided by Dr. T. Onodera. Cells were grown and maintained at 37 °C in MEM supplemented with 10% fetal bovine serum. N2a and HpL3-4 cells were transiently transfected with each construct using a DNA transfection kit (Lipofectamin, Gibco-BRL). Western blot analyses were performed as described [17]. Vanadate (10 μM at 30 °C for 30 min) and AMP-PNP (100 μM and 2 mM at 30 °C for 30 min) treatments were performed according to the previous report [18].

Immunofluorescent microscopy. For indirect immunofluorescence analysis, fluorescent PrP^C-transfected N2a cells were rinsed with PBS with Ca^{2+} and Mg^{2+} (PBS(+)) and then fixed with 10% formalin in 70% PBS(+) for 30 min at room temperature. After four washes with PBS(−), the fixed cells were incubated 10% FBS in PBS(−) for 30 min at room temperature. They were then incubated for 1 h at room temperature with antibodies at desired concentrations. After four washes with PBS(−), the cells were incubated with either Alexa488 (green) Fluor-conjugated anti-rabbit IgG (Molecular Probes) or Alexa594 (red) Fluor-conjugated anti-mouse IgG (Molecular Probes), diluted 1:200 in PBS, for 1 h at room temperature. The stained cells were washed four times with PBS(−) and mounted with SLOW FADE (Molecular Probes). Samples were imaged with Delta-Vision microscopy system (Applied Precision), out of focus light of the visualized images was removed by interactive deconvolution.

Real-time imaging. To observe living cells, cells were cultured on glass-bottomed dishes (Matsunami) in culture medium without phenol red at 30 °C. Images of cells were collected with a Delta Vision Microscopy System (Applied Precision) equipped with an Olympus IX70 through a cooled CCD camera (Quantix-LC, Photometrics). Fluorescence signals were visualized using a quad beam splitter (Chroma) and the following excitation and emission filter 525/50 nm (Chroma).

In vitro motility assay. For cytosol preparations, N2a cells were collected from 9 cm × 10 dishes, washed and suspended in four volumes of PBS, homogenized, and ultracentrifuged. After ultracentrifugation at 100,000*g* for 60 min, supernatants were collected and used for these experiments. Alexa 594-labelled tubulin (Molecular Probe) was polymerized in PEM buffer (35 mM Pipes, pH 7.0, 0.5 mM EGTA, and 0.5 mM $MgCl_2$). Polymerized tubulin, recombinant GFP-PrP, and cytosol (1 mg/ml) were mixed and incubated at 30 °C for 5 min in PEM buffer in the presence of 1 mM ATP. After incubation, samples were spread onto glass-bottom dishes and then observed with the Delta Vision Microscopy System (Applied Precision).

Results

The intracellular trafficking of fluorescent PrP^C was investigated through the real-time imaging in living cells

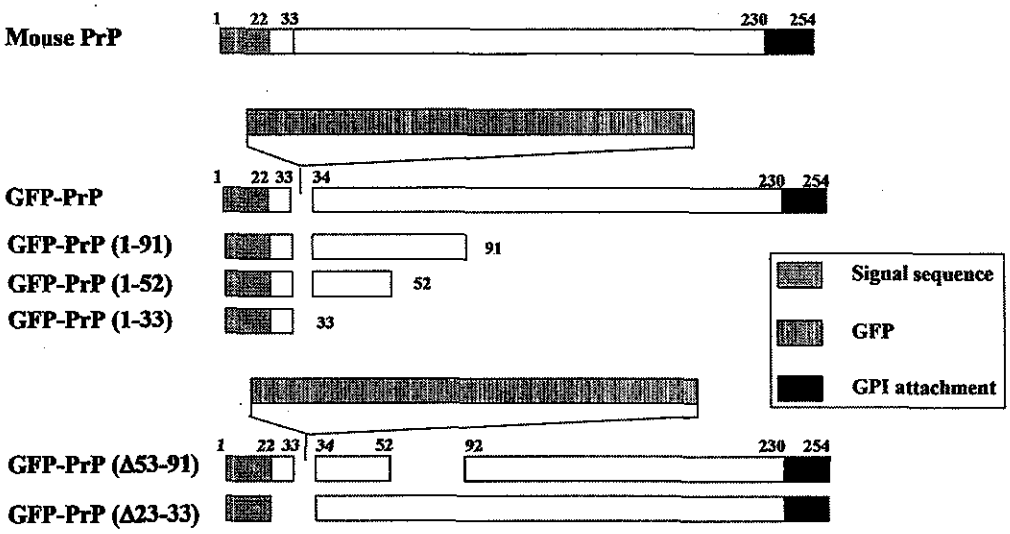

Fig. 1. Immunofluorescent analysis of GFP-PrP^C. The chimeric GFP-PrP constructs including the deletion mutant series used in this study. GFP-PrP (1–91), (1–52), and (1–33) constructs were made as previously described [1]. These recombinant GFP-PrPs were transfected in N2a cells.

by utilizing GFP-PrP constructs (Fig. 1). As results, we revealed that GFP-PrP^C transfected in N2a cells exhibited an anterograde movement towards the direction of plasma membranes at a speed of 140–180 nm/s as well as a retrograde movement inwardly at a speed of 1.0–1.2 μm/s (Fig. 2A). The same results were obtained from other experiments with GFP-PrP^C transfected in HpL3-4 cells (data not shown).

A kinesin family inhibitor of AMP-PNP at a concentration of 100 μM inhibited the anterograde movement of GFP-PrP^C which congregated at an intracellular perinuclear compartment (Fig. 2B), whereas a dynein family inhibitor of vanadate at a concentration of 10 μM inhibited the retrograde movement of GFP-PrP^C which was subsequently detected at the plasma membrane (Fig. 2B) [18]. At a concentration of 2 mM, AMP-PNP inhibited both kinesin and dynein families, and the intracellular motility of GFP-PrP^C was completely blocked (Fig. 2B). The intracellular trafficking of the NH_2-terminal PrP^C fragment was also blocked by the treatment with a microtubule depolymerizer (nocodazole) (data not shown). Furthermore, anti-kinesin antibody (α-kinesin) blocked the anterograde motility of GFP-PrP^C to congregate in an intracellular perinuclear compartment, and anti-dynein antibody (α-dynein) blocked its retrograde motility to reside at a plasma membrane (Fig. 2C).

Next, the deletion mutants (Fig. 1) were used to identify the amino acid residues responsible for the anterograde and retrograde movements of GFP-PrP^C. Truncated constructs with the amino acid residues 1–121, 1–111, and 1–91 in Mo PrP transfected in N2a cells

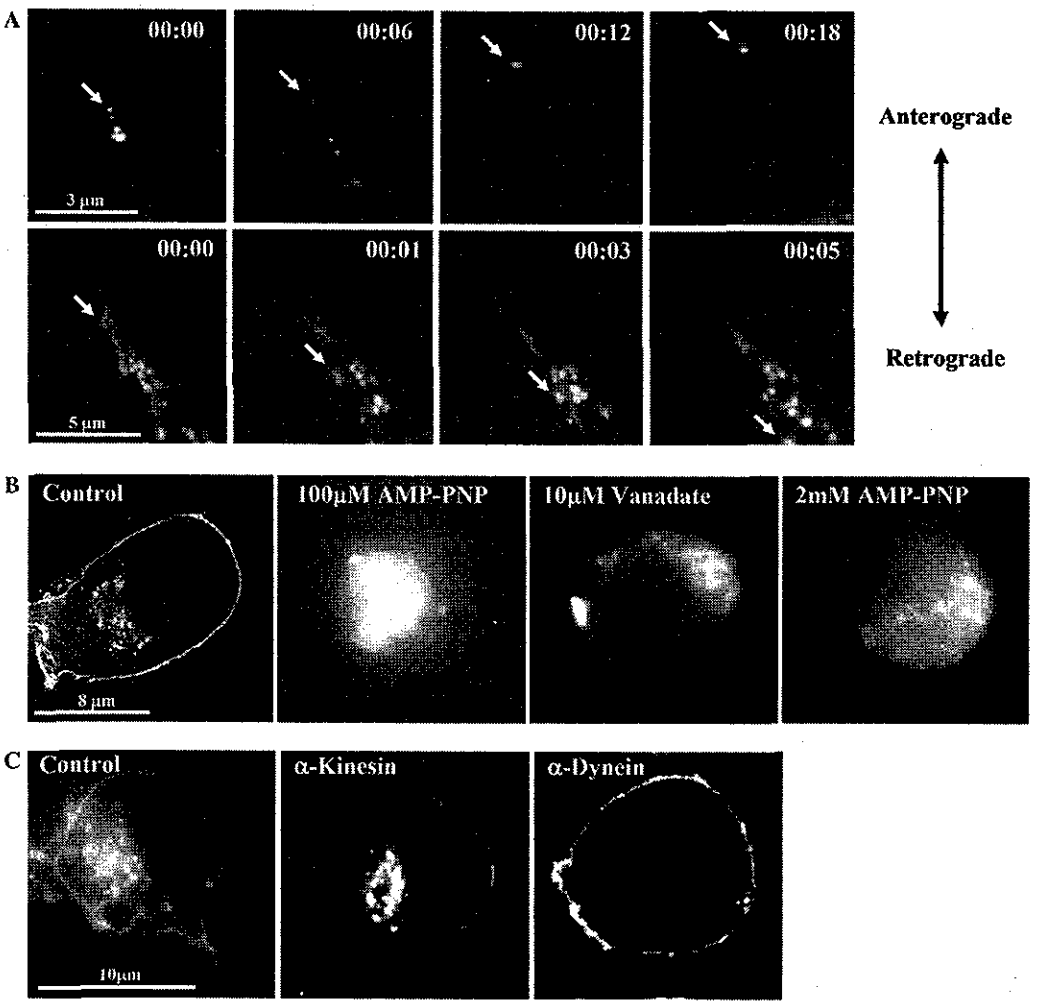

Fig. 2. Intracellular trafficking of GFP-PrP^C by a real-time imaging in living cells, and the drug- or antibody-mediated inhibitions of intracellular movements. (A) Recombinant GFP-PrP^C transfected in N2a cells exhibits an anterograde movement at a speed of 140–180 nm/s (upper panels) and an inward retrograde movement at a speed of 1.0–1.2 μm/s (lower panels). Scale bar (upper panel) = 3 μm and scale bar (lower panel) = 5 μm. (B) A kinesin family inhibitor of AMP-PNP at a concentration of 100 μM inhibited the anterograde movement of GFP-PrP^C which congregates in an intracellular perinuclear compartment. A dynein family inhibitor of vanadate at a concentration of 10 μM inhibits the retrograde movement of GFP-PrP^C which congregates at a plasma membrane. At a concentration of 2 mM, AMP-PNP inhibits both kinesin and dynein families, and the intracellular motility of GFP-PrP^C is completely blocked. Scale bar = 8 μm. (C) Anti-kinesin antibody (α-kinesin) blocks the anterograde motility of GFP-PrP^C and anti-dynein antibody (α-dynein) blocks its retrograde motility.

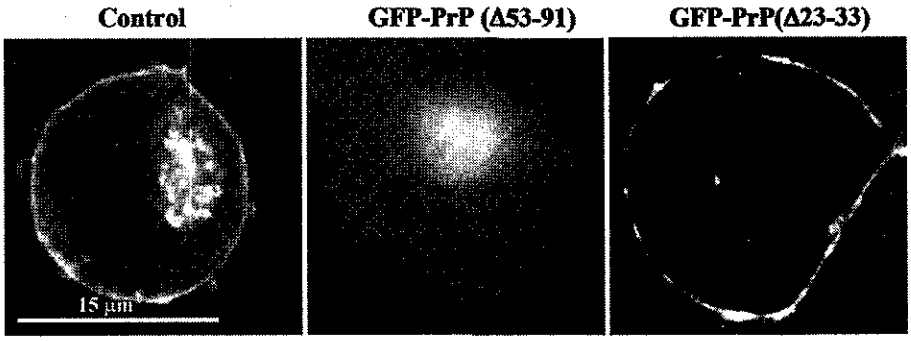

Fig. 3. The amino acid residues responsible for the anterograde and retrograde movements of GFP-PrP^C. The truncated construct of GFP-PrP lacking the amino acid residues 53–91 in Mo PrP loses its anterograde motility and congregates in the intracellular perinuclear compartment. The GFP-PrP construct lacking the amino acid residues 23–33 in Mo PrP loses its retrograde motility and resides at the plasma membrane. Scale bar = 15 μm.

exhibited its proper anterograde and retrograde motilities (data not shown), whereas those with amino acid residues 1–52 and 1–33 in Mo PrP did not [1]. These truncated GFP-PrP^C (1–33 and 1–52) surrounded the γ-tubulin-positive centrosome (microtubule organizing center) (data not shown), suggesting that the truncated GFP-PrP^C with at most 1–52 lost its anterograde movement but those with at least 1–33 still exhibited the dynein-driven retrograde movement. Thus, discrete amino acid residues 53–91 and 23–33 (the first NH2-terminal 1–22 amino acid residues act as a signal sequence) seem to be indispensable for the anterograde and retrograde movements, respectively. In accordance with these observations, the deletion constructs lacking the amino acid residues 53–91 in Mo PrP (GFP-PrP^C (Δ53–91)) lost its anterograde motility and congregated in an intracellular perinuclear compartment, whereas those lacking the amino acid residues 23–33 (GFP-PrP^C (Δ23–33)) lost its retrograde motility and resided at a plasma membrane (Fig. 3).

Finally, an in vitro motility assay [19] was further performed to obtain direct evidence on the interaction at the cytosolic interface between recombinant GFP-PrP and Alexa 594-labelled microtubules with or without cytosolic fractions including kinesin family and dynein motor proteins. However, no movement of GFP-PrP along Alexa 594-labelled microtubules was observed even after the addition of cytosolic fractions (Fig. 4).

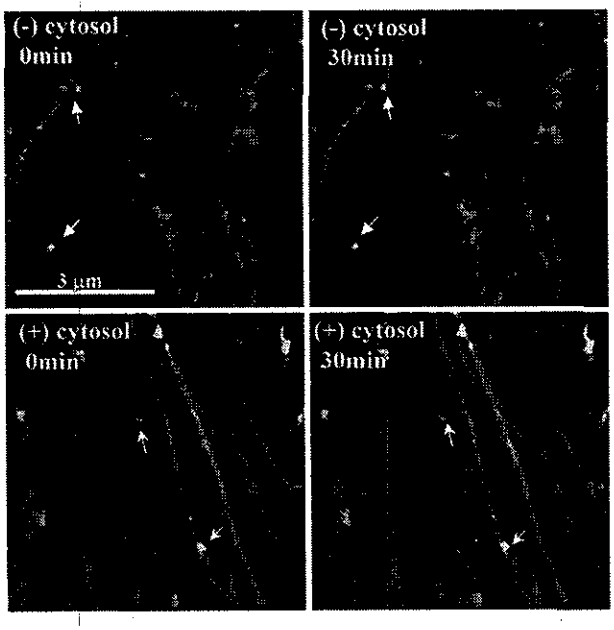

Fig. 4. In vitro motility assay of recombinant GFP-PrP. Polymerized Alexa 594-labelled tubulin, recombinant GFP-PrP, and cytosol (1 mg/ml) were incubated at 30 °C for 5 min in the presence of 1 mM ATP. No movement of recombinant GFP-PrP (arrow heads) along Alexa 594-labelled microtubules was observed for 0–30 min even after the addition of cytosolic fractions (cytosol). Scale bar = 3 μm.

Discussion

We previously reported the microtubule-associated intracellular localization of NH2-terminal PrP^C fragment at a steady state level [1]. A real-time imaging of GFP-PrP^C in living cells, however, has been awaited for further understanding its dynamics along the microtubular network.

Microtubules are essential and ubiquitous cytoskeletal elements composed of heterodimers of α- and β-tubulin, and serve many vital roles, participating in organization of the cytoplasm, in cell motility, and in mitosis [20,21]. In addition to tubulin itself, several microtubule-associated proteins (MAPs) comprise cellular microtubules. The molecular motors that move along microtubules have two origins. The kinesin and myosin families of ATPase motors share a common core structure and may have the same common ancestor as the GTPases involved in signalling and protein synthesis [20,22]. Dynein is part of the family of AAA ATPases [23] that also contribute to protein folding (Hsp100 chaperones), membrane traffic (*N*-ethylmaleimide-sensitive factor or NSF), and DNA synthesis (clamp loader proteins).

Here we showed the anterograde transport of GFP-PrP^C at a speed of 140–180 nm/s and the retrograde transport at a speed of 1.0–1.2 μm/s. These anterograde and retrograde transports of GFP-PrP^C were completely inhibited by AMP-PNP/vanadate which stop the kinesin family/dynein family-driven movements, respectively. Furthermore, anti-kinesin antibody (α-kinesin) blocked the anterograde motility of GFP-PrP^C, and anti-dynein antibody (α-dynein) blocked its retrograde motility. Among the kinesin superfamily, KIF4 moves latex beads from the minus to the plus ends of microtubules, a direction that corresponds to anterograde transport in the axon at a speed of <200 nm/s [24], and dynein is the force-generating protein that produces force in the direction corresponding to retrograde organelle transport at a speed of about 1.4 μm/s in the cell [25–28]. Thus, the anterograde transport of intracellular GFP-PrP^C might be compatible with the speed of the KIF4-driven movement, while the retrograde movement is compatible with that of the dynein-driven movement.

Mapping of the distinct kinesin family-interacting domain and the dynein-interacting domain identified the minimum required amino acid residues in the NH2-terminal PrP^C fragment. The kinesin family-interacting domain (Mo 53–91) is overlapped with an octapeptide repeat region, which is related to the copper metabolism [29–33]. In terms of the PrP^{Sc} formation, the C-terminal domain of PrP^C is known to be insufficient to impede the conversion of the full-length PrP^C molecule to PrP^{Sc} and N-terminally truncated molecules (with residues 23–88 and 23–120 deleted) have reduced dominant-negative activity, and the extreme N-terminal sequence (23KKRPKP29) enhances the dominant-negative phenotype on the formation of PrP^{Sc} [34,35]. This basic sequence is highly conserved in all species studied to date [36]. On the other hand, deletion of the octarepeat sequences (residues 52–91) did not alter PrP^{Sc} formation and dominant-negative inhibition on the formation of PrP^{Sc} [35]. The relevance of these observations to the intracellular trafficking of PrP^C needs to be further investigated.

After internalized, the NH2-terminal PrP^C fragment seems to reside inside vesicles where integral membrane proteins and linker proteins in some cases would be required for the interaction with microtubules to bridge the luminal and cytoplasmic phases across the membranes [1]. Thus, it seems less likely that PrP^C is engaged in the direct interaction with the motor molecules, which is compatible with the fact that the in vitro motility assay failed to show that recombinant GFP-PrP directly moved along Alexa 594-labelled microtubules.

It is also important to identify how many NH2-terminal PrP^C fragments reside in each PrP^C-positive vesicle. In order to answer this question, a single fluorescent molecule is a good potential source because it can emit only one photon at a time. Otherwise it is indispensable to utilize a technique which allows us to know how many photons emit from each PrP^C molecule. Unfortunately, we are currently unable to utilize these techniques. Nonetheless, our results shed a new right on the mechanisms underlying the intracellular trafficking of PrP^C.

Acknowledgments

We greatly thank T. Onodera for providing us the HpL3-4 cell line, E. Nannri, K. Ishibashi, C. Ota, and Y. Yamaura for technical assistance. This work was supported by grants from the Core Research for Evolutional Science and Technology (CREST) of Japan Science and Technology Corporation, Health and Labour Sciences Research Grants, Research on Advanced Medical Technology, nano-001, and the Ministry of Health, Labor and Welfare of Japan.

References

[1] N. Hachiya, K. Watanabe, Y. Sakasegawa, K. Kaneko, Microtubules-associated intracellular localization of the NH2-terminal cellular prion protein fragment, Biochem. Biophys. Res. Commun. 313 (2004) 818–823.
[2] S.B. Prusiner, D.C. Bolton, D.F. Groth, K.A. Bowman, S.P. Cochran, M.P. McKinley, Further purification and characterization of scrapie prions, Biochemistry 21 (1982) 6942–6950.
[3] S.B. Prusiner, P. Peters, K. Kaneko, A. Taraboulos, V. Lingappa, F.E. Cohen, S.J. DeArmond, Cell Biology of Prions, Cold Spring Harbor, New York, 1999.
[4] A. Taraboulos, M. Scott, A. Semenov, D. Avrahami, L. Laszlo, S.B. Prusiner, Cholesterol depletion and modification of COOH-terminal targeting sequence of the prion protein inhibit formation of the scrapie isoform, J. Cell Biol. 129 (1995) 121–132.
[5] M. Rogers, D. Serban, T. Gyuris, M. Scott, T. Torchia, S.B. Prusiner, Epitope mapping of the Syrian hamster prion protein utilizing chimeric and mutant genes in a vaccinia virus expression system, J. Immunol. 147 (1991) 3568–3574.
[6] K.-M. Pan, N. Stahl, S.B. Prusiner, Purification and properties of the cellular prion protein from Syrian hamster brain, Protein Sci. 1 (1992) 1343–1352.
[7] S.-L. Shyng, J.E. Heuser, D.A. Harris, A glycolipid-anchored prion protein is endocytosed via clathrin-coated pits, J. Cell Biol. 125 (1994) 1239–1250.
[8] S.-L. Shyng, K.L. Moulder, A. Lesko, D.A. Harris, The N-terminal domain of a glycolipid-anchored prion protein is essential for its endocytosis via clathrin-coated pits, J. Biol. Chem. 270 (1995) 14793–14800.
[9] M. Nunziante, S. Gilch, H.M. Schatzl, Essential role of the prion protein N terminus in subcellular trafficking and half-life of cellular prion protein, J. Biol. Chem. 278 (2003) 3726–3734.
[10] K.S. Lee, A.C. Magalhaes, S.M. Zanata, R.R. Brentani, V.R. Martins, M.A. Prado, Internalization of mammalian fluorescent cellular prion protein and N-terminal deletion mutants in living cells, J. Neurochem. 79 (2001) 79–87.
[11] A.C. Magalhaes, J.A. Silva, K.S. Lee, V.R. Martins, V.F. Prado, S.S.G. Ferguson, M.V. Gomez, R.R. Brentani, M.A.M. Prado, Endocytic intermediates involved with the intracellular trafficking of a fluorescent cellular prion protein, J. Biol. Chem. 277 (2002) 33311–33318.
[12] A. Negro, C. Ballarin, A. Bertoli, M.L. Massimino, M.C. Sorgato, The metabolism and imaging in live cells of the bovine prion

protein in its native form or carrying single amino acid substitutions, Mol. Cell. Neurosci. 17 (2001) 521–538.
[13] H. Lorenz, O. Windl, H.A. Kretzschmar, Cellular phenotyping of secretory and nuclear prion proteins associated with inherited prion diseases, J. Biol. Chem. 277 (2002) 8508–8516.
[14] L. Ivanova, S. Barmada, T. Kummer, D.A. Harris, Mutant prion proteins are partially retained in the endoplasmic reticulum, J. Biol. Chem. 276 (2001) 42409–42421.
[15] D.A. Butler, M.A. Scott, J.M. Bockman, D.R. Borchelt, A. Taraboulos, K.K. Hsiao, D.T. Kingsbury, S.B. Prusiner, Scrapie-infected murine neuroblastoma cells produce protease-resistant prion proteins, J. Virol. 62 (1988) 1558–1564.
[16] C. Kuwahara, A.M. Takeuchi, T. Nishimura, K. Haraguchi, A. Kubosaki, Y. Matsumoto, K. Saeki, T. Yokoyama, S. Itohara, T. Onodera, Prions prevent neuronal cell-line death, Nature 400 (1999) 225–226.
[17] M.R. Scott, R. Kohler, D. Foster, S.B. Prusiner, Chimeric prion protein expression in cultured cells and transgenic mice, Protein Sci. 1 (1992) 986–997.
[18] T.A. Schroer, M.P. Sheetz, Role of kinesin and kinesin-associated proteins in organelle transport, in: F.D. Warner, J.R. McIntosh (Eds.), Cell Movement, Alan R. Liss, New York, 1989, pp. 295–306.
[19] A. Kubo, H. Sasaki, A. Yuba-Kubo, S. Tsukita, N. Shiina, Centriolar satellites: molecular characterization, ATP-dependent movement toward centrioles and possible involvement in ciliogenesis, J. Cell Biol. 147 (1999) 969–980.
[20] T.D. Pollard, The cytoskeleton, cellular motility and the reductionist agenda, Nature 422 (2003) 741–745.
[21] J. Howard, A.A. Hyman, Dynamics and mechanics of the microtubule plus end, Nature 422 (2003) 753–758.
[22] R.D. Vale, R.A. Milligan, The way things move: looking under the hood of molecular motor proteins, Science 288 (2000) 88–95.
[23] G. Mocz, I.R. Gibbons, Model for the motor component of dynein heavy chain based on homology to the AAA family of oligomeric ATPases, Structure (Camb) 9 (2001) 93–103.
[24] N. Hirokawa, Kinesin and dynein superfamily proteins and the mechanism of organelle transport, Science 279 (1998) 519–526.
[25] R.D. Vale, B.J. Schnapp, T. Mitchison, E. Steuer, T.S. Reese, M.P. Sheetz, Different axoplasmic proteins generate movement in opposite directions along microtubules in vitro, Cell 43 (1985) 623–632.
[26] R.D. Vale, T.S. Reese, M.P. Sheetz, Identification of a novel force-generating protein, kinesin, involved in microtubule-based motility, Cell 42 (1985) 39–50.
[27] B.M. Paschal, R.B. Vallee, Retrograde transport by the microtubule-associated protein MAP 1C, Nature 330 (1987) 181–183.
[28] R.B. Vallee, J.S. Wall, B.M. Paschal, H.S. Shpetner, Microtubule-associated protein 1C from brain is a two-headed cytosolic dynein, Nature 332 (1988) 561–563.
[29] D.R. Brown, K. Qin, J.W. Herms, A. Madlung, J. Manson, R. Strome, P.E. Fraser, T. Kruck, A. von Bohlen, W. Schulz-Schaeffer, A. Giese, D. Westaway, H. Kretzschmar, The cellular prion protein binds copper in vivo, Nature 390 (1997) 684–687.
[30] P.C. Pauly, D.A. Harris, Copper stimulates endocytosis of the prion protein, J. Biol. Chem. 273 (1998) 33107–33110.
[31] M.L. Kramer, H.D. Kratzin, B. Schmidt, A. Romer, O. Windl, S. Liemann, S. Hornemann, H. Kretzschmar, Prion protein binds copper *within* the physiological concentration range, J. Biol. Chem. 276 (2001) 16711–16719.
[32] W.S. Perera, N.M. Hooper, Ablation of the metal ion-induced endocytosis of the prion protein by disease-associated mutation of the octarepeat region, Curr. Biol. 11 (2001) 519–523.
[33] A.P. Garnett, J.H. Viles, Copper binding to the octarepeats of the prion protein. Affinity, specificity, folding, and cooperativity: insights from circular dichroism, J. Biol. Chem. 278 (2003) 6795–6802.
[34] K. Kaneko, L. Zulianello, M. Scott, C.M. Cooper, A.C. Wallace, T.L. James, F.E. Cohen, S.B. Prusiner, Evidence for protein X binding to a discontinuous epitope on the cellular prion protein during scrapie prion propagation, Proc. Natl. Acad. Sci. USA 94 (1997) 10069–10074.
[35] L. Zulianello, K. Kaneko, M. Scott, S. Erpel, D. Han, F.E. Cohen, S.B. Prusiner, Dominant-negative inhibition of prion formation diminished by deletion mutagenesis of the prion protein [In Process Citation], J. Virol. 74 (2000) 4351–4360.
[36] P. Bamborough, H. Wille, G.C. Telling, F. Yehiely, S.B. Prusiner, F.E. Cohen, Prion protein structure and scrapie replication: theoretical, spectroscopic, and genetic investigations, Cold Spring Harb. Symp. Quant. Biol. 61 (1996) 495–509.

Non-glycosylphosphatidylinositol (GPI)-anchored recombinant prion protein with dominant-negative mutation inhibits PrP^{Sc} replication *in vitro*

Hitaru Kishida[1,2], Yuji Sakasegawa[1,3], Kota Watanabe[1,3], Yoshio Yamakawa[4], Masahiro Nishijima[4], Yoshiyuki Kuroiwa[2], Naomi S. Hachiya[1,3] and Kiyotoshi Kaneko[1,3]

1. Department of Cortical Function Disorders, National Institute of Neuroscience, National Center of Neurology and Psychiatry, Kodaira, Tokyo, Japan
2. Department of Neurology, Yokohama City University, Yokohama, Japan
3. Core Research for Evolutional Science and Technology (CREST), Japan Science and Technology Corporation, Kawagoe, Saitama, Japan
4. Department of Biochemistry and Cell Biology, National Institute of Infectious Diseases, Tokyo, Japan

KEY WORDS: recombinant prion protein (rPrP), dominant negatives, Q218K, quinacrine, glycosylphosphatidylinositol (GPI)-anchor, lipid rafts, Creutzfeldt-Jakob disease (CJD)

ABBREVIATIONS: PrP = prion protein, GPI = glycosylphosphatidylinositol, CJD = Creutzfeldt-Jakob disease, rPrP = recombinant prion protein, EC_{50} = 50% effective concentration, EC_{99} = 99% effective concentration, PrP^{C} = host-encoded cellular prion protein, PrP^{Sc} = abnormal protease-resistant pathogenic prion protein, TSE = transmissible spongiform encephalopathy, BSE = bovine spongiform encephalopathy, IPTG = Isopropyl-β-D-thiogalactopyranoside, β-ME = β-mercaptoethanol, PMSF = Phenylmethylsulfonyl fluoride, PBS = phosphate buffer saline, PK = proteinase K, WST-8 = 2- (2-methoxy-4-nitrophenyl)- 3- (4-nitrophenyl)- 5- (2,4-disulfophenyl)- 2H- tetrazolium, monosodium salt, SPR = surface plasmon resonance, PIPLC = phosphatidyl-inositol specific phospholipase C

Abstract

Dominant-negative mouse prion protein (PrP) with a lysine mutation at codon 218 (Q218K) is known to inhibit prion replication. In order to gain further mechanistic insight into such dominant negative inhibition, non-glycosylphosphatidylinositol (GPI)-anchored recombinant PrP with Q218K (rPrP-Q218K) was investigated. When applied into scrapie-infected mouse neuroblastoma (ScN2a) cells, rPrP-Q218K but not wild-type rPrP (rPrP-WT) exclusively inhibited abnormal protease-resistant pathogenic isoform (PrP^{Sc}) replication without reducing the viability of the cells. It was even more efficient than quinacrine, which has already been prescribed for sporadic Creutzfeldt-Jakob disease (CJD) patients; 50% effective concentration (EC_{50}) = 0.20 μM, 99% effective concentration (EC_{99}) = 0.86 μM vs. EC_{50} = 0.45 μM, EC_{99} = 1.5 μM. Besides, no apparent cell damage was observed at the concentration of up to 4.3 μM (100 μg/ml). In combination treatment with 0.43 μM (10 μg/ml) of rPrP-Q218K, EC_{99} of quinacrine was decreased from 1.5 μM to 0.5 μM, and the cell viability was recovered from 50% to over 90% as inversely proportional to the concentration of quinacrine. Such combination could alleviate the side effects of quinacrine by reducing its effective concentration without changing or even acceleration the inhibition efficacy. Since homogeneous, high-quality rPrPs could be easily prepared from Escherichia coli in large quantities, rPrP-Q218K is a good candidate for a prion replication antagonist.

Correspondence: Dr. Kiyotoshi Kaneko, MD, Department of Cortical Function Disorders, National Institute of Neuroscience, National Center of Neurology and Psychiatry, 4-1-1 Ogawahigashi Kodaira, Tokyo 187-8502, Japan
Tel: 81-42-346-1718 Fax: 81-42-346-1748 E-mail: kaneko@ncnp.go.jp

Submitted: July 14, 2003 Revision Accepted: October 22, 2003

DOI: 10.1080/13506120410001689634

Introduction

Human prion disease or transmissible spongiform encephalopathy (TSE), such as sporadic Creutzfeldt-Jakob disease (CJD) and variant CJD transmitted from bovine spongiform encephalopathy (BSE) constitutes a group of invariably fatal neurodegenerative disorders[1,2]. Prion protein (PrP) consists of two isoforms, one is a host-encoded cellular isoform (PrP^{C}) and the other is an abnormal protease-resistant pathogenic isoform (PrP^{Sc}). The latter is a causative agent of prion disease. PrP^{Sc} stimulates the conversion of PrP^{C} into nascent PrP^{Sc}, and the accumulation of PrP^{Sc} leads to the central nervous system (CNS) dysfunction and neuronal degeneration[3].

A human polymorphic lysine variant at codon 219 (E219K) in the Japanese population, known to render humans resistant to sporadic *CJD*[4,5], acts as a *dominant* negative in scrapie-infected mouse neuroblastoma (ScN2a) culture cells after gene transfection[6,7] and transgenic mice expressing lysine at codon 218 in mouse PrP (mouse Q218K, which corresponds to human E219K)[8]. Of note, such a genetic population with E219K and the transgenic mice with Q218K complete their life span with no apparent phenotypic abnormality[5,8].

We now demonstrate that administration of non-glycosylphosphatidylinositol (GPI)-anchored recombinant PrP (rPrP) with Q218K mutation (rPrP-Q218K) but not wild-type rPrP (rPrP-WT) exclusively inhibited the PrP^{Sc} formation in ScN2a cells, even more efficiently than quinacrine, which has already been prescribed for CJD patients, and no apparent cell damage was observed up to 5-fold higher concentrations of a 99% effective concentration (EC_{99}). When combined, rPrP-Q218K efficiently reduced the effective dosage of quinacrine, and thus rendered ScN2a culture cells more viable. Such a combination could alleviate the side effects of quinacrine by reducing its effective concentration without changing or even accelerating the inhibition efficacy. Since homogeneous, high-quality rPrP could be easily prepared from *Escherichia coli* in large quantities, rPrP-Q218K might be a good candidate as a prion replication antagonist.

Materials and methods

Expression plasmid construction

The gene, mouse (Mo) PrP(23-230), coding for residues 23-230 of mouse PrP was PCR-amplified from mouse brain cDNA using the oligonucleotide primers (5′-GGAATTCACCATGAAAAAGCGGCCAAAGCCTGGAGGG-3′ and 5′-CCGCTCGAGTCAGGATCTTCTCCCGTCGTAATAGGC-3′) and cloned via *EcoRI* and *XhoI* sites into the plasmid pBluescript II SK(+) (Stratagene, La Jolla, CA). The genes for 3F4-tagged MoPrP (*MHM2PrP*) were also cloned using PCR amplification from pSPOX-MHM2PrP[9,10] as above. The Q218K mutation was generated by PCR-directed mutagenesis using primers (5′-ATGTGCGTCACCCAGTACAAAAAGGAGTCC-3′ and 5′-ATAGGCCTGGGACTCCTTTTTGTACTGGGT-3′). The DNA fragments were cloned into a modified pET-11a (Invitrogen, Carlsbad, CA), pEY2, of which *EcoRI* and *XhoI* sites were introduced as multi-cloning sites, via *EcoRI* and *XhoI* sites.

Purification of recombinant prion proteins (rPrPs)

The rPrPs were expressed as inclusion bodies in the *E. coli* BL21(DE3) (Stratagene) in the presence of 0.1 mM Isopropyl-β-D-thiogalactopyranoside (IPTG). The inclusion bodies were collected from sonicated lysates by centrifugation at 27,000 × g for 10 min, washed three times in Buffer A (2 M urea, 50 mM Tris-HCl, pH 7.5, 150 mM NaCl, 2 mM β-mercaptoethanol (β-ME), 0.5 mM Phenylmethylsulfonyl fluoride (PMSF)), and solubilized in Buffer B (8 M urea, 25 mM Tris-HCl, pH 7.5, 2 mM β-ME, 0.5 mM PMSF). After centrifugation (200,000 × g, 30 min), the supernatant was applied to a CM-Sepharose column (Amersham Bioscience, Piscataway, NJ), washed with Buffer B containing 100 mM NaCl and eluted with Buffer B containing 150 mM NaCl. The eluate containing rPrP was applied to an Ni-NTA agarose column (Qiagen, Valencia, CA), washed with Buffer B containing 5 mM imidazole and eluted with Buffer B containing 200 mM imidazole. The eluate was diluted 10-fold 1 M arginine-HCl, pH 8.0, 1 mM reduced glutathione, 0.8 mM oxidized glutathione and incubated at 4°C overnight. After incubation at 37°C for 10 min, the refolded recombinant proteins were concentrated and buffer-changed into phosphate buffer saline (PBS) by Ultrafree-15 10K NMWL (Millipore, Billerica, MA). Concentrations of rPrP were calculated by the absorbance at 280 nm with specific absorbance unit ($A_{280nm,\ 1mg/ml,\ 1cm}$) of 2.70.

Inhibition assay of PrP^{Sc} accumulation in ScN2a cells

ScN2a cells were grown and maintained as described[11]. Twenty-four hours after splitting, cells were incubated in a fresh medium containing the appropriate concentration of rPrP and/or quinacrine (Sigma, St. Louis, MO) or the same volume of PBS as a negative control and incubated for 3 days. Quinacrine was dissolved in PBS. Cell lysis and proteinase K (PK) digestion were performed as described[12]. PK-insoluble pellets and PK-undigested samples were subjected to 12% SDS-PAGE and Western blotting using standard procedure. Anti-PrP

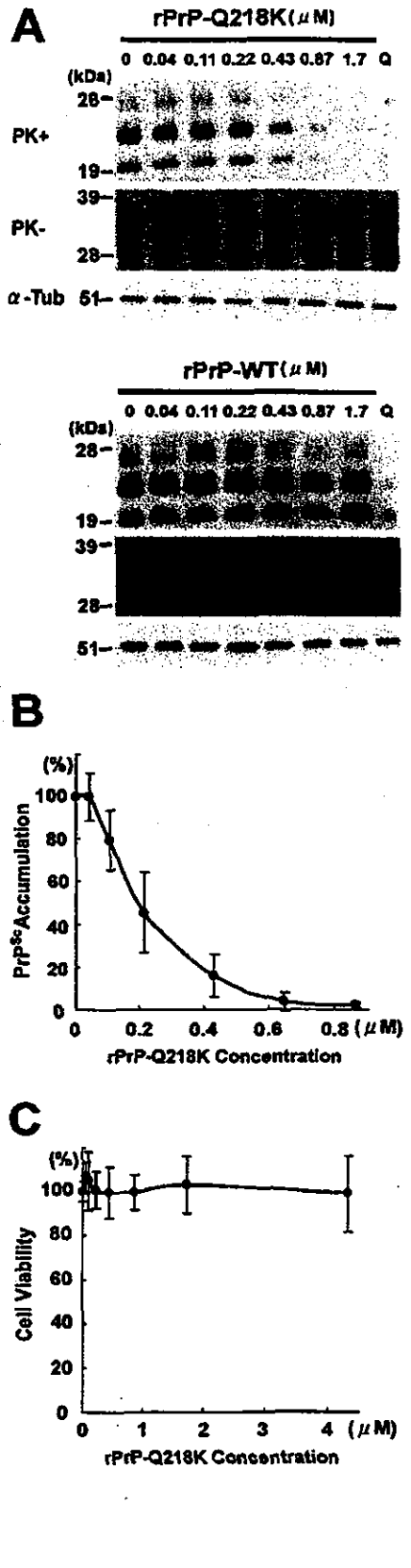

monoclonal antibody (mAb) 6H4 (1:5000; Prionics, Schlieren, Switzerland) or α-tubulin mAb (1:10000; DM1A, Sigma) was used as the primary antibody, and horseradish peroxydase-conjugated anti-mouse IgG (1:5000; Cappel, West Chester, PA) was used as the secondary antibody. Immunodecorated bands were visualized by the ECL-plus (Amersham Bioscience). For evaluating the accumulation of PrP^{Sc}, the PK-resistant bands were quantified by densitometry (LAS-1000; Fujifilm, Tokyo, Japan). Average values of at least three independent experiments were plotted as percentage of the amount of PrP^{Sc} found in equivalent untreated ScN2a cells on the day of collection.

Cytotoxicity assays

The cytotoxicity of rPrP and quinacrine in ScN2a cells was evaluated by the WST-8 assay (Cell Counting Kit-8, Dojindo Lab, Kumamoto, Japan) measuring the formation of a yellow color formazan dye produced by dehydrogenase activities in viable cells from 2- (2-methoxy-4-nitrophenyl)- 3- (4-nitrophenyl)- 5- (2,4-disulfophenyl)- 2H- tetrazolium, monosodium salt (WST-8). ScN2a cells (4×10^{3} cells/well) were cultured at 37°C for 24 h in 96-well plates, incubated in the medium containing the appropriate concentration of drugs for 48 h and were subjected to WST-8 assay according to the manufacturer's protocol.

FIGURE 1: Dose-dependent inhibition of PrP^{Sc} formation in ScN2a cells with rPrP-Q218K. (A) PrP^{Sc} signals in ScN2a culture cells are compared by immunoblotting in the presence of rPrP-Q218K or rPrP-WT at 0 – 1.7 μM (0 - 40 μg/ml). (0) represents untreated cells, and (Q) represents positive controls treated with 1.5 μM of quinacrine. PrP^{Sc} is detected with anti-PrP mAb (6H4) after proteinase K (PK) digestion (20 μg/ml, 1 h, 37°C, 1st row), and total PrP (PrP^{C} and PrP^{Sc}) is detected without PK digestion (2nd row). After incubation with rPrP-Q218K, PrP^{Sc} in ScN2a cells is reduced in a dose-dependent manner, whereas the administration of rPrP-WT by up to 1.7 μM (40 μg/ml) does not change PrP^{Sc} formation. Total PrP remains unchanged in both treatments. The same undigested cell lysates are stained with αtubulin mAb (DM1A, Sigma, St. Louis, MO). (B) Densitometric measurements of PrP^{Sc} signals in panel A. All data represent the mean values (± SD) from at least three independent experiments. (C) Cell viability is determined by the WST-8 assay, in which the absorbance values indicate the yield of colored formazan in proportion to total number of viable cells. Each point represents the mean absorbance value (± SD) calculated from four sets of experimental data. Up to 4.3 μM (100 μg/ml) of rPrP-Q218K doesn't reduce the viability of ScN2a cells.

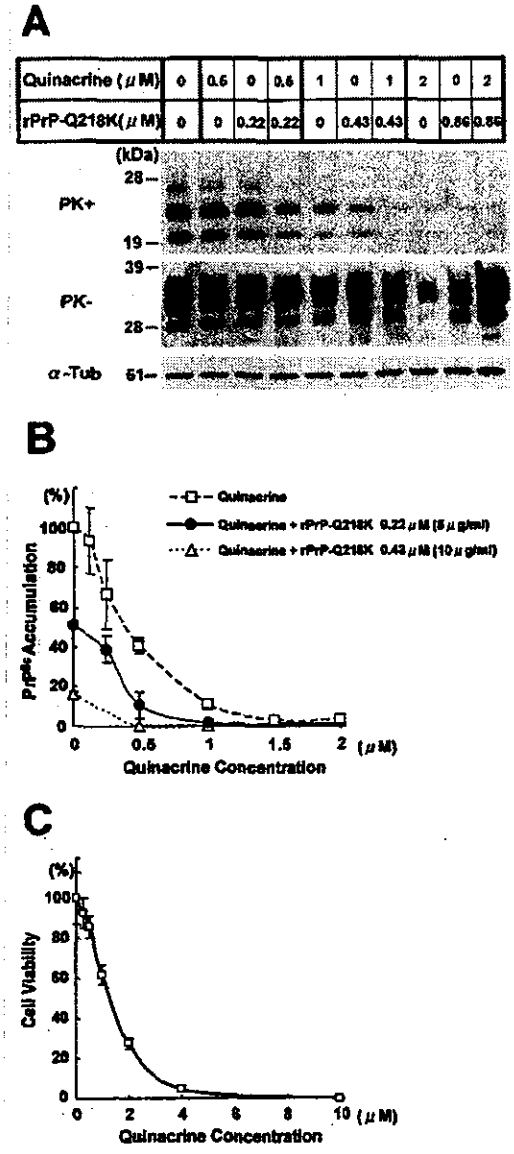

FIGURE 2: Additive inhibition of PrP^{Sc} formation by the combination of rPrP-Q218K and quinacrine. (A) PrP^{Sc} signals in ScN2a cells are compared by immunoblotting in the presence of quinacrine and/or rPrP-Q218K (see legend to Figure. 1A). PrP^{Sc} level in ScN2a cells is additively reduced. (B) Densitometric measurements of PrP^{Sc} signals in panel A (see legend to Figure. 1B). Open squares, quinacrine; filled circles, quinacrine with 0.22 μM (5 μg/ml) of rPrP-Q218K; open triangles, quinacrine with 0.43 μM (10 μg/ml) of rPrP-Q218K. The inhibition on PrP^{Sc} formation with quinacrine with rPrP-Q218K is more effective than that of quinacrine alone. (C) Cell viability is determined by the WST-8 assay (see legend to Figure. 1C). The treatment of quinacrine damages the cell viability in a dose-dependent manner.

Immunofluorescent microscopy

For indirect immunofluorescence analysis, mouse neuroblastoma (N2a) cells grown on glass cover slips in the presence of 0.43 μM (10 μg/ml) of rPrP with 3F4 epitope (MHM2 rPrP) for 3 h were rinsed with PBS without Ca^{2+} and Mg^{2+} (PBS(−)) and then fixed with 2% formalin in 70% PBS(−) for 15 min at room temperature. After four washes, the fixed cells were incubated 10% FBS in PBS(−) for 30 min at room temperature. They were then incubated for 1 h at room temperature with anti-SHaPrP 3F4 mAb (1:200; Sigma) and anti-asialo-GM1 antibody (1:200, CALBIOCHEM, La Jolla, CA) as a marker of rafts. After four washes with PBS (−), the cells were incubated with Alexa 488 Fluor-conjugated goat anti-mouse IgG (1:500, Molecular Probes, Eugene, OR) and Alexa 594 Fluor-conjugated goat anti-rabbit IgG (1:100, Molecular Probes) for 1 h at room temperature. The cells were washed 4 times with PBS(−) and mounted with SLOW FADE (Molecular Probes) and observed using Delta Vision Microscope Systems (Applied Precision, LLC).

Surface plasmon resonance (SPR) measurement

A BIAcore 3000 system (BIAcore AB, Uppsala, Sweden) was used to analyze molecular interactions by means of SPR. rPrP-WT at 500 μg/ml was diluted 1:10 with 10 mM sodium acetate buffer at pH 6.0 and immobilized to a sensor chip CM5 (carboxymethylated dextran surface) using amine coupling according to the manufacture's instructions. Samples for analyte proteins were diluted ($3.2 \times 10^{-2 \sim 0}$ μg/ml) in the running buffer (10 mM HEPES-KOH, pH 7.4, 150 mM NaCl, 3 mM EDTA, 0.005% Surfactant P20), and injected over the surface at 4°C with a flow rate of 20 μl/min. Each sensorgram was subtracted for the response observed in the control flow cell containing a blank surface and results were analyzed by using BIA evaluation SPR kinetic software (BIAcore).

Results

Purified rPrP-Q218K or rPrP-WT was added into the culture media of ScN2a cells at the designated concentrations and incubated for 3 days (see Materials and methods). Ultracentrifugation using a sucrose density gradient revealed that these rPrPs were monomeric (data not shown). While PrP^{Sc} formation was not altered by up to 1.7 μM (40 μg/ml) of rPrP-WT (Figure 1A), it was dramatically reduced in rPrP-Q218K-treated ScN2a cells; 50% effective concentration (EC_{50}) was 0.19 μM (4.5 μg/ml) and EC_{99} was 0.86 μM (20 μg/ml) (Figure 1B) in a concentration-dependent manner (Figures 1A, 1B). Of

note, the viability of ScN2a cells measured with WST-8 assay was not reduced up to 5-fold higher concentrations than EC_{99} of rPrP-Q218K (Figure 1C). On the contrary, quinacrine reduced viability of ScN2a cells by 50% at the concentration of EC_{99} (1.5 μM) (Figure 2C). As previously demonstrated[13,14], quinacrine inhibited PrP^{Sc} formation in ScN2a cells (EC_{50}=0.45 μM, EC_{99}= 1.5 μM) but less efficiently.

When both rPrP-Q218K and quinacrine were applied onto ScN2a cells simultaneously, an additive inhibitory effect was observed. After the combined administration of 0.5 μM of quinacrine and 0.22 μM (5 μg/ml) of rPrP-Q218K, PrP^{Sc} formation in ScN2a cells was reduced by another 30% compared with quinacrine alone (Figure 2A, 2B). When combined with 0.43 μM (10 μg/ml) of rPrP-Q218K, EC_{99} of quinacrine was also decreased from 1.5 μM to 0.5 μM, in which the cell viability was recovered from 50% to over 90% as inversely proportional to the concentration of quinacrine (Figure 2C).

In order to gain further mechanistic insight into the inhibition of PrP^{Sc} formation by rPrP-Q218K, morphological and biochemical analyses were performed. Indirect immunofluorescent microscopy detected these rPrPs on the cell surface with no difference in distribution profiles (Figure 3). These results show that some factor/s other than the GPI-anchor rendered the rPrPs detected on the cell surface.

SPR measurement revealed that both analytes of rPrP-Q218K and rPrP-WT did not bind to rPrP-WT immobilized onto the chip surface as a ligand, whereas anti-prion mAb 6H4 bound the ligand of rPrP at the equilibrium dissociation constant (K_D) of 2.2 x 10^{-9}. In order to correct the instrumental noise and non-specific binding, the sensorgram of the flow cell containing rPrP-WT-immobilized sensor chip was subtracted from that of a blank cell. However, SPR could not detect any interaction between amine-coupled rPrP-WT on the surface of the chip and soluble rPrP-Q218K/rPrP-WT in the flow, indicating their KD values below the detection limit of SPR measurement.

Discussion

While mouse Q218K in a GPI-anchored form has already been known as a dominant negative in ScN2a culture cells[6,7] and transgenic mice[8], we have demonstrated that the administration of non-GPI-anchored rPrP-Q218K sufficiently inhibits PrP^{Sc} formation in ScN2a cells for the first time.

Meier *et al.* recently reported that soluble wild-type PrP derivatives might represent a new class of prion replication antagonists with transgenic and gene knockout approaches[15]. In PrP transgenic mice with a wild-type background, the expression of PrP^{C} rendered soluble and dimeric by fusion to immunoglobulin Fcγ (PrP-Fc2) delays PrP^{Sc} accumulation, agent replication, and onset of disease following inoculation with infective prions. While it is preliminary to consider such gene therapeutics, *e.g.* an *ex vivo* gene transfer approach[16,17], the direct administration of soluble rPrPs such as our rPrP-Q218K would be an alternative approach for prion therapeutics. In addition, homogeneous and high-quality soluble rPrP-Q218K could be easily prepared from large-scale fermentation of *E. coli* in sufficient quantities.

Artificial administration of anti-PrP antibodies have been shown to exert a protective effect against infection with PrP^{Sc} [18, 19], which is in good agreement with our own data *in vitro*; EC_{50} of anti-PrP antibody Fab D18 (kindly provided by Dr. Stanley B. Prusiner)=6 nM, and EC_{99}=30 nM (data not shown). However, a recent clinical trial of Aβ vaccination targeting Alzheimer's disease has been halted due to the serious neurological complications of autoimmune reactions developing in

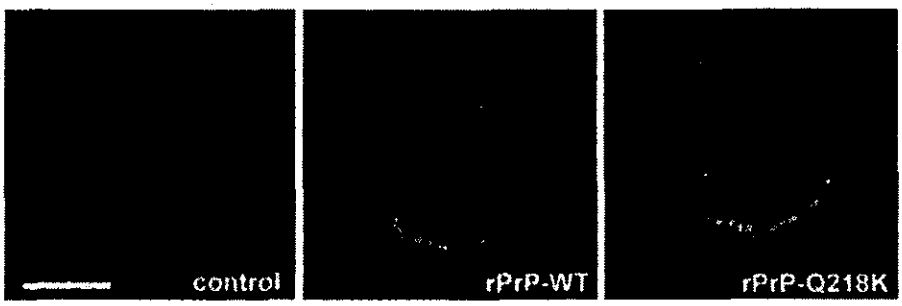

FIGURE 3: Both rPrP-WT and rPrP-218K bind to N2a cells. N2a cells are incubated for 3 h with PBS(−), 10 μg/ml rPrP-WT or rPrP-Q218K, washed with PBS(−), fixed with 2% formalin, and subjected to indirect immunofluorescent microscopy. rPrPs, asialo-GM1 are displayed in green and red, respectively. PrP^{C} and asialo-GM1 are localized on the plasma membrane. Both rPrPs are detected on a part of lipid rafts. Bar: 15 μm.

some patients[20,21]. In contrast, the generation of anti-PrP antibodies *in vivo* has proven quite difficult in wild-type animals, PrP being a notoriously poor immunogen[22]. From the aspect of avoiding such unwanted autoimmune reactions, rPrPs might also be considered as a better candidate for prion therapeutics.

Quinacrine, an anti-malarial drug, was reported to inhibit PrP^{Sc} formation in ScN2a cells[13,14], and has already been prescribed for CJD patients in a tentative way[23]. Unfortunately, quinacrine tends to provoke a drug-induced liver dysfunction[24], which frequently forces cessation of the drug administration. In order to minimize the side effects of quinacrine, we expected that combination treatment of multiple anti-prion drugs might be an alternative option. In fact, when combined with rPrP-Q218K, the EC_{99} of quinacrine was successfully reduced and no significant cytotoxicity was observed at the same range of concentration in ScN2a cells. Such a combination could alleviate the side effects of quinacrine by reducing its effective concentration without changing or even accelerating the inhibition efficacy.

Enari *et al.*[25] proposed that sequestration of PrP^{C} by anti-PrP antibody or removal by phosphatidyl-inositol specific phospholipase C (PIPLC) leads to depletion of PrP^{Sc} due to much more rapid turnover of PrP^{Sc} than previously supposed. Since decrease in PrP^{C} by administration of rPrP-Q218K to ScN2a cells was not detected (Figure 1A), the inhibition of PrP^{Sc} accumulation seems to be caused by secession of PrP^{Sc} synthesis, stimulation of PrP^{Sc} degradation or a combination of both.

It was shown that both rPrP-Q218K and rPrP-WT in non-GPI-anchored form were equally detectable on the cell surface, where the conversion of PrP^{C} into PrP^{Sc} takes place[26,27]. Of note, such equal binding seems to be independent of the inhibition of PrP^{Sc} formation, since only rPrP-Q218K but not rPrP-WT exclusively inhibited the PrP^{Sc} formation in ScN2a cells. Nonetheless, one might assume that rPrP-Q218K aberrantly binds to endogenous PrP^{C} in terms of the binding partner, which is undetectable by the conventional immunofluorescent microscopy, and concurrently inhibits PrP^{Sc} formation. Real-time kinetics analysis by SPR, however, failed to detect any significant difference in the binding kinetics of rPrP-WT as a ligand with rPrP-WT or rPrP-Q218K as analytes. Measurements of on-rates (ka) and off-rates (kd) of protein-protein interactions made by SPR is extremely sensitive, and these values are directly related to KD[28]. Taken into account the fact that SPR successfully detects binding interactions in the order of 10^{-3}~$^{-4}$ of KD[28], it seems less likely that such discrepancy between rPrP-Q218K and rPrP-WT on the PrP^{Sc} inhibition could be explained by the different binding kinetics of these rPrPs against PrP, although rPrP may not perfectly substitute for PrP^{C}. Instead, it seems likely that these rPrPs more readily interact with a binding factor/s other than PrP where rPrP-Q218K and rPrP-WT are equally detected but inhibit PrP^{Sc} formation differently. Legname *et al.*[29] recently reported that the dominant-negative MoPrP (MoPrP-Q218K)-Fc, in which the C-terminus of MoPrP was fused to the Fc portion of an IgG, not only binds to granule cells but also binds to neurons of the molecular layer where PrP^{C} is expressed, and assuming that the cells of the molecular layer express an auxiliary protein/s, provisionally designated protein X[6,30], which is involved in prion replication. Identification of such factor/s remains to be further examined.

Acknowledgments

We thank Drs. Naoko Iwanami, Yuko Nakamura, and Ken'ichi Hagiwara for useful discussions and Dr. Tamaki Muramoto for providing ScN2a culture cells. This work was supported in part by grants from the Ministry of Health, Labor and Welfare of Japan (14161301), and Core Research for Evolutional Science and Technology (CREST), Japan Science and Technology Corporation.

References

1 Prusiner SB (2001). Shattuck lecture—neurodegenerative diseases and prions. *N Engl J Med* 344, 1516-1526
2 Collinge J (1999). Variant Creutzfeldt-Jakob disease. *Lancet* 354, 317-323
3 Prusiner SB (1998). Prions. *Proc Natl Acad Sci USA* 95, 13363-13383
4 Kitamoto T and Tateishi J (1994). Human prion diseases with variant prion protein. *Philos Trans R Soc Lond B* 343, 391-398
5 Shibuya S, Higuchi J, Shin RW, Tateishi J and Kitamoto T (1998). Codon 219 Lys allele of PRNP is not found in sporadic Creutzfeldt-Jakob disease. *Ann Neurol* 43, 826-828
6 Kaneko K, Zulianello L, Scott M, Cooper CM, Wallace AC, James TL, Cohen FE and Prusiner SB (1997). Evidence for protein X binding to a discontinuous epitope on the cellular prion protein during scrapie prion propagation. *Proc Natl Acad Sci USA* 94, 10069-10074
7 Zulianello L, Kaneko K, Scott M, Erpel S, Han D, Cohen FE and Prusiner SB (2000). Dominant-negative inhibition of prion formation diminished by deletion mutagenesis of the prion protein. *J Virol* 74, 4351-4360
8 Perrier V, Kaneko K, Safar J, Vergara J, Tremblay P, DeArmond SJ, Cohen FE, Prusiner SB and Wallace AC (2002). Dominant-negative inhibition of prion replication in transgenic mice. *Proc Natl Acad Sci USA* 99,13079-13084

9 Scott MR, Köler R, Foster D and Prusiner SB (1992). Chimeric prion protein expression in cultured cells and transgenic mice. *Protein Sci* **1**, 986-997

10 Rogers M, Serban D, Gyuris T, Scott M, Torchia T and Prusiner SB (1991). Epitope mapping of the Syrian hamster prion protein utilizing chimeric and mutant genes in a vaccinia virus expression system. *J Immunol* **147**, 3568-3574

11 Butler DA, Scott MA, Bockman JM, Borchelt DR, Taraboulos A, Hsiao KK, Kingsbury DT and Prusiner SB (1988). Scrapie-infected murine neuroblastoma cells produce protease-resistant prion proteins. *J Virol* **62**, 1558-1564

12 Korth C, Kaneko K and Prusiner SB (2000). Expression of unglycosylated mutated prion protein facilitates PrP(Sc) formation in neuroblastoma cells infected with different prion strains. *J Gen Virol* **81**, 2555-2563

13 Doh-Ura K, Iwaki T and Caughey B (2000). Lysosomotropic agents and cysteine protease inhibitors inhibit scrapie-associated prion protein accumulation. *J Virol* **74**, 4894-4897

14 Korth C, May BCH, Cohen FE and Prusiner SB (2001). Acridine and phenothiazine derivatives as pharmacotherapeutics for prion disease. *Proc Natl Acad Sci USA* **98**, 9836-9841

15 Meier P, Genoud N, Prinz M, Maissen M, Rulicke T, Zurbriggen A, Raeber AJ and Aguzzi A (2003). Soluble dimeric prion protein binds PrP(Sc) *in vivo* and antagonizes prion disease. *Cell* **113**, 49-60

16 Corbel SY and Rossi FM (2002). Latest developments and in vivo use of the Tet system: ex vivo and in vivo delivery of tetracycline-regulated genes. *Curr Opin Biotechnol* **13**, 448-452

17 Kapturczak MH, Flotte T and Atkinson MA (2001). Adeno-associated virus (AAV) as a vehicle for therapeutic gene delivery: improvements in vector design and viral production enhance potential to prolong graft survival in pancreatic islet cell transplantation for the reversal of type 1 diabetes. *Curr Mol Med* **1**, 245-258

18 Peretz D, Williamson RA, Kaneko K, Vergara J, Leclerc E, Schmitt-Ulms G, Mehlhorn IR, Legname G, Wormald MR, Rudd PM, Dwek RA, Burton DR and Prusiner SB (2001). Antibodies inhibit prion propagation and clear cell cultures of prion infectivity. *Nature* **412**, 739-743

19 White AR, Enever P, Tayebi M, Mushens R, Linehan J, Brandner S, Anstee D, Collinge J and Hawke S (2003). Monoclonal antibodies inhibit prion replication and delay the development of prion disease. *Nature* **422**, 80-83

20 Dodart JC, Bales KR and Paul SR (2003). Immunotherapy for Alzheimer's disease: will vaccination work? *Trends Mol Med* **9**, 85-87

21 McGeer PL and McGeer E (2003). Is there a future for vaccination as a treatment for Alzheimer's disease? *Neurobiol Aging* **24**, 391-395

22 Koller MF, Grau T and Christen P (2002). Induction of antibodies against murine full-length prion protein in wild-type mice. *J Neuroimmunol* **132**, 113-116

23 Follette P (2003). New perspectives for prion therapeutics meeting. Prion disease treatment's early promise unravels. *Science* **299**, 191-192

24 Scoazec JY, Krolak-Salmon P, Casez O, Besson G, Thobois S, Kopp N, Perret-Liaudet A and Streichenberger N (2003). Quinacrine-induced cytolytic hepatitis in sporadic Creutzfeldt-Jakob disease. *Ann Neurol* **53**, 546-547

25 Enari M, Flechsig E and Weissmann C (2001). Scrapie prion protein accumulation by scrapie-infected neuroblastoma cells abrogated by exposure to a prion protein antibody. . *Proc Natl Acad Sci USA* **98**, 9295-9299

26 Taraboulos A, Scott M, Semenov A, Avrahami D, Laszlo L and Prusiner SB (1995). Cholesterol depletion and modification of COOH-terminal targeting sequence of the prion protein inhibit formation of the scrapie isoform. *J Cell Biol* **129**, 121-132

27 Kaneko K, Vey M, Scott M, Pilkuhn S, Cohen FE and Prusiner SB (1997). COOH-terminal sequence of the cellular prion protein directs subcellular trafficking and controls conversion into the scrapie isoform. *Proc Natl Acad Sci USA* **94**, 2333-2338

28 Myszka DG (1997). Kinetic analysis of macromolecular interactions using surface plasmon resonance biosensors. *Curr Opin Biotechnol* **8**, 50-57

29 Legname G., Nelken P, Guan Z, Kanyo ZF, DeArmond SJ and Prusiner SB (2002). Prion and doppel proteins bind to granule cells of the cerebellum. *Proc Natl Acad Sci USA* **99**, 16285-16290

30 Telling GC, Scott M, Mastrianni J, Gabizon R, Torchia M, Cohen FE, DeArmond SJ and Prusiner SB (1995). Prion propagation in mice expressing human and chimeric PrP transgenes implicates the interaction of cellular PrP with another protein. *Cell* **83**, 79-90

Available online at www.sciencedirect.com
SCIENCE DIRECT®
Biochemical and Biophysical Research Communications 319 (2004) 78–82
BBRC
www.elsevier.com/locate/ybbrc

Interaction of D-lactate dehydrogenase protein 2 (Dld2p) with F-actin: implication for an alternative function of Dld2p

Naomi S. Hachiya,[a,b,c] Yuji Sakasegawa,[a,c] Akiko Jozuka,[a,b] Shoichiro Tsukita,[c,d,e] and Kiyotoshi Kaneko[a,b,*]

[a] *Department of Cortical Function Disorders, National Institute of Neuroscience (NIN), National Center of Neurology and Psychiatry (NCNP), Tokyo 187-8502, Japan*
[b] *Core Research for Evolutional Science and Technology (CREST), Japan Science and Technology Agency, Saitama 332-0012, Japan*
[c] *Tsukita Cell Axis Project, Exploratory Research for Advanced Technology (ERATO), Japan Science and Technology Corporation, Saitama 332-0012, Japan*
[d] *Department of Cell Biology, Faculty of Medicine, Kyoto University, Kyoto 606-8501, Japan*
[e] *Solution Oriented Research for Science and Technology (SORST), Japan Science and Technology Corporation, Saitama 332-0012, Japan*

Received 5 April 2004
Available online 12 May 2004

Abstract

D-Lactate dehydrogenase protein 2 [Yeast 15 (1999) 1377; Biochem. Biophys. Res. Commun. 295 (2002) 910] was initially identified as the actin interacting protein 2 (Aip2p) using a two-hybrid screen to search for proteins that interact with actin [Nat. Struct. Biol. 2 (1995) 28], but no other evidence indicating an interaction between Aip2p and actin cytoskeleton has been reported so far. During our search for the protein conformation modifying activity, we serendipitously identified Aip2p isolated from *Saccharomyces cerevisiae* as exhibiting an interaction with F-actin both in vitro and in vivo. Incubation with Aip2p facilitated the formation of the circular form of F-actin in vitro, which exhibited an aberrant trypsin susceptibility. Overexpression of Aip2p induced multi-buds in yeast cells, whereas reduced expression interfered with the formation of the cleavage furrow for the cell division, which was rescued by the introduction of wild-type Aip2p. While Aip2p-treated F-actin in the circular form was negligibly stained by rhodamine-labeled phalloidin (rhodamine–phalloidin) in vitro, rhodamine–phalloidin staining profiles in actin interacting protein 2 gene (AIP2)-modified cells suggested a correlation between the conformation of F-actin and the expression of Aip2p in vivo. AIP2-deleted cells became sensitive to osmotic conditions, a hallmark of actin dysfunction. Finally, immunoprecipitation of yeast cells using anti-Aip2p antibody demonstrated that Aip2p associates with actin. These properties suggest that Aip2p may interact with F-actin in vivo and play an important role in the yeast cell morphology.

Keywords: D-Lactate dehydrogenase protein 2; Actin interacting protein 2; Actin interacting protein 2 gene; F-actin; Trypsin susceptibility assay; Rhodamine–phalloidin staining; Yeast cell morphology

The actin cytoskeleton plays diverse roles in the cell, mediating endocytosis, exocytosis, cell motility, cell polarity, and cytokinesis, each in a spatially localized and temporally controlled manner [4]. Each of these events requires regulation of specific dynamic properties and spatial organization of actin filaments by members of a large collection of actin-binding proteins.

Actin interacting protein 1 (Aip1p) was originally identified using a two-hybrid screen, which has a distinct interaction footprint on actin subdomains III and IV, and is required for normal localization of cofilin to cortical actin patches as well as stimulation of cofilin activity [5]. Aip1p has also been proposed to control actin depolymerization in vivo, and plays an important regulatory role in the rapid remodeling of the cortical actin meshwork [6]. The crystal structure of Aip1p from *Saccharomyces cerevisiae* (*S. cerevisiae*) reveals that overall folding is mediated by two connected

* Corresponding author. Fax: +81-42-346-1748.
E-mail address: kaneko@ncnp.go.jp (K. Kaneko).

0006-291X/$ - see front matter © 2004 Elsevier Inc. All rights reserved.
doi:10.1016/j.bbrc.2004.04.146

seven-bladed propellers [7]. The gene (YDL178w) encoding actin interacting protein 2 (Aip2p) was also identified using a two-hybrid screen to search for *S. cerevisiae* proteins that interact with actin [3], but there has been no direct evidence indicating an in vivo interaction between Aip2p and actin cytoskeleton so far. Subsequently, the YDL178w gene product has been reported to localize on mitochondria and exhibit D-lactate dehydrogenase (DLD) activity in vitro, and therefore renamed as D-lactate dehydrogenase protein 2 (Dld2p) [1]. The AIP3 gene encodes actin interacting protein 3 (Aip3p), which is identical to BUD6 that functions in bipolar bud selection in yeast diploid cells [8–10]. Aip3p is not essential for mitotic growth but is necessary for normal morphogenesis, and plays an important role in actin-directed polarized cell growth in yeast cells.

We previously developed an in vitro protein conformation modifying assay that measures the factor-dependent increase in protease susceptibility of a substrate as a criterion for activity [11–13]. Serendipitously, we isolated a chaperone that alters the conformation of protein substrates such as F-actin in vitro. This purified chaperone is the Aip2p [1,3]. The activity of the isolated Aip2p could alter the conformation of F-actin in vitro and the rhodamine–phalloidin staining profiles as well as its osmotic sensitivity in vivo, which seems to be involved in yeast cell morphology.

Materials and methods

Yeast strains and antibodies. Wild-type yeast strains (ATCC24657 for the wild-type strain, ATCC96099 and ATCC 96100 were mated for the diploid cells) used in this study were purchased from American Type Culture Collection. Protease deficient strain SH2777 was a gift from Dr. Harashima, Osaka University. Anti-actin antibody was purchased from Chemicon. Anti-Aip2p antibody was raised against the synthetic peptide corresponding to the C-terminal 15 amino acid residues of Aip2p (VHYDPNGILNPYKYI) which were coupled through a COOH-terminal cysteine residue to BSA.

Purification of hexahistidine-tagged Aip2p. In an effort to obtain sufficient quantities of Aip2p, the protein was prepared from the expression strain in yeast under control of the ADH promoter. The C-terminally hexahistidine-tagged YDL178w gene was amplified by PCR and inserted into the aureobasidin A (Ab A) selective expression vector pAUR123 (TaKaRa Biomedicals). The protease deficient strain SH2777 was transformed by this plasmid and transformants were grown on YPD plates containing 0.5 μg ml^{-1} Ab A. Inoculated medium (8 L) was incubated overnight at 30 °C to an OD at 600 nm of 1–2. Cells were collected, resuspended in 4 volumes of buffer B (50 mM NaPi (pH 8.0), 150 mM NaCl, and 10 mM imidazole), crushed using glass beads, and centrifuged at 10,000 rpm for 10 min at 4 °C. Supernatants were collected and ultracentrifuged at 100,000*g* at 4 °C for 1 h. The precipitate was resuspended, passed through a Ni–NTA agarose column (Qiagen, K.K.) equilibrated in buffer B, and subsequently eluted with buffer B containing 0.5 M imidazole. Eluted fractions were dialyzed against buffer C (10 mM Hepes–KOH (pH 7.4), 50 mM NaCl, and 1 mM DTT), applied to an ion exchange Mono Q column (Amersham–Pharmacia Biotech, AKTA system) equilibrated with buffer C, and eluted with a linear NaCl gradient (100–500 mM). Immunoreactive fractions were dialyzed against buffer D (50 mM NaPi (pH 7.5), 10 mM NaCl, and 1 mM Mg $(OAc)_2$), and finally passed through a Superdex 200 gel filtration column equilibrated with buffer D.

Fluorescent microscopy. Rhodamine-labeled phalloidin (rhodamine–phalloidin) staining was performed as previously [14]. Samples were imaged with a Delta-Vision microscopy system (Applied Precision), with out of focus light pertaining to visualized images being removed by interactive deconvolution.

Formation of circular F-actin in vitro. Alexa 488-labeled G-actin (Molecular Probes) was converted into its Mg^{2+} form and polymerized for 2 h. Purified histidine-tagged Aip2p was added to Alexa 488-conjugated F-actin in the buffer E (10 mM Tris–Cl (pH 8.0), 0.1 M KCl, and 10 mM $MgCl_2$) and then incubated at 30 °C for 30 min in the presence of 1 mM ATP. Twenty microliter samples were then placed onto a glass-bottomed dish and covered with Slow fade anti-fade (Molecular Probes). To observe a staining profile of the circular F-actin with anti-Aip2p antibody, Alexa 594-conjugated anti-Aip2p antibody (red) was incubated with Alexa 488-conjugated F-actin (green). Affinity-purified Alexa 594-conjugated anti-Aip2p antibody was used at 1:100.

Trypsin susceptibility assay. Assays (200 μl) were initiated by adding 200 ng of polymerized rabbit muscle actin to buffer E containing 1 mM ATP and 500 ng of hexahistidine-tagged Aip2p, and incubated at 30 °C for 15 min. After incubation, samples were treated with trypsin (0.2 μg ml^{-1}) at 16 °C for 15 min. The reaction was terminated by incubation with soybean trypsin inhibitor (0.4 μg ml^{-1}) on ice for 5 min, TCA-precipitated with tRNA carrier, and then subjected to SDS–PAGE and Western blotting. To detect actin, affinity-purified polyclonal rabbit anti-actin antibody served as the primary antibody and horseradish peroxidase-linked IgG (ICN Pharmaceuticals) was the secondary antibody. Immunoreactive bands were visualized by ECL-plus (Amersham Biosciences) and analyzed using a Fluoro Smax (Bio-Rad).

Overexpression and disruption of actin interacting protein 2 gene in yeast cells. In an effort to obtain an Aip2p overexpressed strain, a cloned actin interacting protein 2 gene (AIP2) encoding Aip2p was inserted into the galactose inducible yeast expression vector pYES2. Yeast cells (ATCC96099) were transformed by this plasmid, selected on minimal plates without uracil, and checked by colony PCR. Aip2p was induced with 2% galactose at 30 °C for 6 h. To generate a strain containing a disrupted AIP2, the middle region of Aip2p (1039 base pairs) was substituted with a histidine marker gene fragment, and then inserted into pBluescript KS+ vector (Stratagene). A diploid strain was transformed with the linearized vector and the tetrads produced were then analyzed by Southern blotting to verify the presence of the disrupted gene.

Immunoprecipitation of Aip2p–actin complex. Yeast spheroplasts from wild-type or AIP2-deleted cells were gently homogenized in the buffer (10 mM Tris–Cl, pH 8.0, 0.1 M KCl, and 10 mM $MgCl_2$) followed by an centrifugation at 100,000*g* for 60 min at 4 °C. An antibody against the C-terminal peptide of Aip2p or an antibody against yeast actin (Chemicon) was conjugated to Formyl-cellulofine (Seikagaku-Kogyo) according to the manufacturer's instructions. The resin was equilibrated with immunoprecipitation buffer (20 mM Tris–HCl, pH 7.9, 75 mM KCl, 0.5 mM EDTA, 0.5 mM EGTA, and 8% sucrose) and then used for the immunoprecipitation.

Results

Aip2p–F-actin interaction in vitro

In the absence of Aip2p, polymerized F-actin displayed a linear structure (Fig. 1A, (−) Aip2p), whereas in the presence of Aip2p, de novo formation of circular F-actin was observed (Fig. 1A, (+) Aip2p). The average

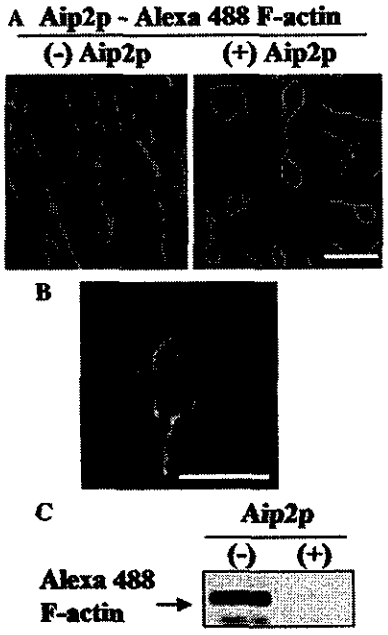

Fig. 1. (A) Formation of circular F-actin in vitro. Alexa 488-conjugated actin (Molecular Probes) was polymerized in high salt buffer (10 mM Tris–Cl (pH 8.0), 100 mM KCl, and 2 mM $MgCl_2$) and incubated with or without Aip2p in the presence of 1 mM ATP. Scale bar is 5 μm. (B) Anti-Aip2p antibody stains the circular F-actin in a discontinuous pattern. Alexa 594-conjugated anti-Aip2p antibody (red) was incubated with Alexa 488-conjugated F-actin (green) as described in Materials and methods. Samples were examined by fluorescent microscopy. Scale bar is 5 μm. (C) Trypsin susceptibility of Aip2p-bound circular F-actin is increased. Alexa 488-conjugated F-actin was incubated with Aip2p and ATP as described in Materials and methods. Samples were examined by fluorescent microscopy and subjected to the trypsin susceptibility assay.

radius of the circular F-actin was approximately 2–4 μm, which remained constant under the reaction conditions used in this study (Aip2p:F-actin = 1:1–1:5) (data not shown). The circularization process was very efficient as over 60% of the F-actin changed into circular form after incubation with Aip2p at 30 °C for 30 min. Alexa 488-conjugated anti-Aip2p antibody stained the circular F-actin in a discontinuous pattern (Fig. 1B). Incubation of Alexa 488-conjugated F-actin with Aip2p did not increase the rate of G-actin (see Fig. 1A). Alexa 488-conjugated F-actin was incubated with or without Aip2p as described above, treated with trypsin, and then subjected to Western blot analysis. The protease susceptibility of the Aip2p-bound "circular form" of F-actin clearly increased (Fig. 1C), indicating that the Aip2p-bound "circular form" of F-actin possesses an aberrant conformation compared to the linear form of F-actin.

Altered yeast cell morphology after the AIP2 modification

The phenotypic abnormalities were observed following modification of AIP2 expression. When Aip2p was overexpressed in yeast cells using the multicopy expression vector pYES2 and cultured under Aip2p-inducible conditions, cells produced multi-buds from the same mother neck or exhibited elongated bud necks (Fig. 2A, Overexpressed). This suggested that an excessive amount of Aip2p resulted in an abnormal budding process in yeast cells. In contrast, AIP2-deleted cells displayed deformed morphology reflecting an inability to properly form the cleavage furrow during cell division (Fig. 2A, Disrupted). The expression of intact Aip2p in the AIP2-deleted cells rescued this morphological defect (Fig. 2A, Plasmid rescue (AIP2)).

Because an abnormal actin cytoskeleton is considered as a major cause of such altered yeast cell morphology [15], the distribution of F-actin was examined in wild-type yeast cells, AIP2-deleted cells, and AIP2-overexpressed cells using rhodamine–phalloidin staining, which specifically stains F-actin in yeast cells. F-actin

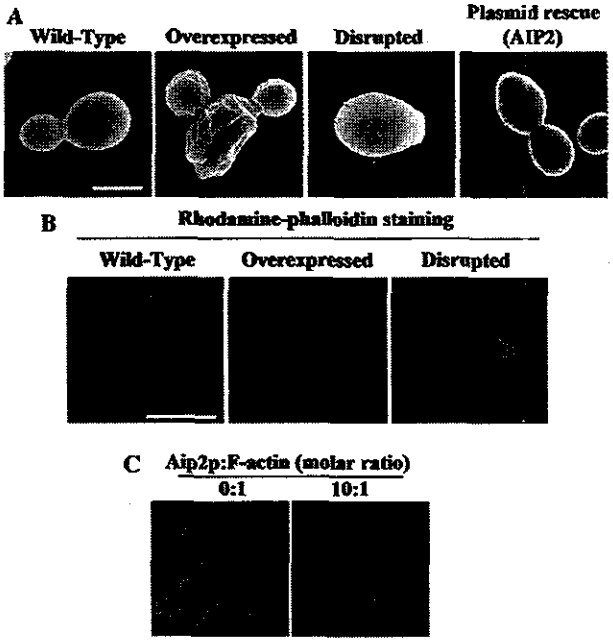

Fig. 2. (A) Wild-type (Wild-Type), AIP2-overexpressed (Overexpressed), and AIP2-deleted (Disrupted) strains were visualized using scanning electron microscopy (SEM). AIP2-overexpressed yeast cells produced multi-buds, while AIP2-deleted cells could not generate a proper cleavage furrow. The expression of AIP2 restored the cell morphology defect of the deleted strain (Plasmid rescue, AIP2). The AIP2-deleted strain was transformed with the pAUR123 plasmid carrying the gene for Aip2p under control of the ADH promoter. All transformants were cultured to an OD of 0.5–0.8 at 600 nm and then observed with SEM. Scale bar is 2 μm. (B) F-actin distribution with or without Aip2p in vivo. Wild-type yeast (Wild-Type), AIP2-deleted cells (Disrupted), and AIP2-overexpressed cells (Overexpressed) were incubated with 6.6 μM of rhodamine–phalloidin (red). Yeast cell wall was counterstained by Calcofluor White (Sigma) shown as blue. (C) F-actin distribution with or without Aip2p in vitro. Rabbit muscle actin (Molecular Probes) was polymerized, incubated with (10:1) or without (0:1) Aip2p in the presence of 1 mM ATP, and then stained with 6.6 μM of rhodamine–phalloidin.

was found to be clustered in the AIP2-deleted cells (Fig. 2B, right panel, Disrupted) compared to wild-type cells (Fig. 2B, left panel, Wild-Type). In contrast, when Aip2p was overexpressed in the wild-type strain using a multicopy expression vector, rhodamine–phalloidin-stained F-actin was only sparsely observed (Fig. 2B, middle panel, Overexpressed).

The in vitro rhodamine–phalloidin staining profile of F-actin on a glass slide varied considerably from that of F-actin incubated with Aip2p. Rhodamine–phalloidin hardly detected F-actin following incubation with Aip2p (Fig. 2C, right panel, 10:1) compared to the rhodamine–phalloidin staining profile of F-actin in the absence of Aip2p (Fig. 2C, left panel, 0:1). When fluorescently labeled G-actin was polymerized and used as a substrate (Alexa 488-conjugated F-actin), on the other hand, the fluorescent signals were not altered even after the incubation with Aip2p (see Fig. 1A). The total F-/G-actin contents remained at the same level after the AIP2-modification (data not shown).

Taken together, the incubation with Aip2p either competitively interferes with the rhodamine–phalloidin staining of F-actin or modifies the conformation of F-actin which the rhodamine–phalloidin hardly stained. The fact that the in vitro formation of circular F-actin (Fig. 1A) with its modified trypsin susceptibility (Fig. 1C) after the incubation with Aip2p supports the latter notion. Furthermore, the AIP2-deleted cells became sensitive to osmotic conditions (Fig. 3A), which is a hallmark of actin dysfunction [15]. Finally, immunoprecipitation of yeast cells using anti-Aip2p antibody demonstrated that Aip2p associates with actin (Fig. 3B, left panel). The reciprocal immunoprecipitation experiment using anti-actin antibody showed that Aip2p is contained in a complex with anti-actin antibody (Fig. 3B, right panel).

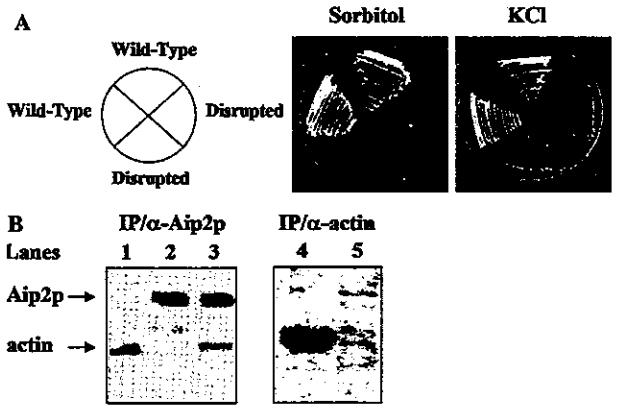

Fig. 3. (A) AIP2-deleted cells are osmotic sensitive. Wild-type (Wild-Type) and AIP2-deleted cells (Disrupted) were grown on rich media containing 1.8 M sorbitol or 1.2 M KCl at 30 °C. (B) Actin and Aip2p were detected by anti-actin antibody (α-actin, lanes 1, 3, and 4) and anti-Aip2p antibody (α-Aip2p, lanes 2, 3, and 5), respectively, in the complex immunoprecipitated with anti-Aip2p antibody (IP/α-Aip2p, lane 3), and in the complex immunoprecipitated with anti-actin antibody (IP/α-actin, lanes 4 and 5). Lanes 1 (actin) and 2 (Aip2p) are marker lanes.

Discussion

A two-hybrid screen originally identified the AIP2 that interacts with actin in *S. cerevisiae* proteins, and therefore it was classified as a member of actin interacting proteins [3]. Chelstowska et al. [1] reported that cell extracts expressing Aip2p exhibited DLD activity in vitro and renamed as D-lactate dehydrogenase protein 2 (Dld2p), even though its expression was not dependent on the Rtg proteins, which are known to be required for the expression of the CIT2 gene that encodes the peroxysomal isoform of citrate synthase. Flick and Konieczny [2] also found Aip2p, implicated with potential MLP/CRP3 interacting proteins, from a mouse cDNA library and exhibited DLD activity in vitro. It is well known that DLD activity is found in mitochondrial fractions. Nevertheless, the interaction between actin cytoskeleton and Aip2p has not been characterized by these efforts.

Given that Aip2p was initially identified as a member of actin interacting protein, several lines of evidence detailing the interaction between Aip2p and actin cytoskeleton were obtained and consisted of: (1) Aip2p-bound F-actin adopted a circular form with a resultant increase in trypsin susceptibility in vitro; (2) rhodamine–phalloidin-stained F-actin congregated in AIP2-deleted cells, however, when Aip2p was overexpressed using a multicopy expression vector, rhodamine–phalloidin-stained F-actin was only sparsely distributed; and (3) AIP2-deleted cells became osmotically sensitive. Schwikowski et al. [16] suggested that the function of Aip2p may be associated with cell polarity by a computational analysis of protein–protein interactions in yeast, which seems to be consistent with our results. It is possible that Dld2p/Aip2p may be multifunctional.

The actin cytoskeleton is relatively flexible compared to microtubules. With regard to in vitro actin manipulation, Ishiwata and colleagues [17] reported a laborious approach that established the formation of a super helix/circular form of F-actin in their motility assay system in which polymerized F-actin was bound to a silicone- or nitrocellulose-coated surface on which a torque component using heavy meromyosin and ATP was assembled to slide F-actin. Even in their well-defined system, formation of the super helix/circular form was determined by chance based on the balance between the magnitude of net torque and the rigidity of the actin filament. Consequently, circular F-actin is not easily produced. In contrast, we achieved the formation of circular F-actin simply by incubating the linear

conformer with Aip2p in the presence of ATP in vitro, a process that was 60–70% efficient over 30 min.

In this study, we have demonstrated that the Aip2p interacts with actin cytoskeleton. Moreover, our results provide the first evidence that Aip2p activity is involved in yeast cell morphology. Disruption or overexpression of the AIP2 significantly affected bud formation in yeast cells, which indicates that Aip2p is required for proper yeast cell morphology. The properties we have identified suggest that a more complete understanding of the activities of Aip2p may facilitate the analysis of the mechanisms that regulate F-actin dynamics in vivo.

Acknowledgments

We greatly thank Y. Kozuka for the technical tutorial and T. Hirai for his assistance. This work was supported by grants from the Core Research for Evolutional Science and Technology (CREST) of Japan Science and Technology Corporation, Health and Labour Sciences Research Grants, Research on Advanced Medical Technology, nano-001, The Naito Foundation, and the Ministry of Health, Labor and Welfare of Japan.

References

[1] A. Chelstowska, Z. Liu, Y. Jia, D. Amberg, R.A. Butow, Signalling between mitochondria and the nucleus regulates the expression of a new D-lactate dehydrogenase activity in yeast, Yeast 15 (1999) 1377–1391.

[2] M.J. Flick, S.F. Konieczny, Identification of putative mammalian D-lactate dehydrogenase enzymes, Biochem. Biophys. Res. Commun. 295 (2002) 910–916.

[3] D.C. Amberg, E. Basart, D. Botstein, Defining protein interactions with yeast actin in vivo, Nat. Struct. Biol. 2 (1995) 28–35.

[4] T.D. Pollard, The cytoskeleton, cellular motility and the reductionist agenda, Nature 422 (2003) 741–745.

[5] A.A. Rodal, J.W. Tetreault, P. Lappalainen, D.G. Drubin, D.C. Amberg, Aip1p interacts with cofilin to disassemble actin filaments, J. Cell Biol. 145 (1999) 1251–1264.

[6] A. Konzok, I. Weber, E. Simmeth, U. Hacker, M. Maniak, A. Muller-Taubenberger, DAip1, a *Dictyostelium* homologue of the yeast actin-interacting protein 1, is involved in endocytosis, cytokinesis, and motility, J. Cell Biol. 146 (1999) 453–464.

[7] W.C. Voegtli, A.Y. Madrona, D.K. Wilson, The structure of Aip1p, A WD repeat protein that regulates cofilin-mediated actin depolymerization, J. Biol. Chem. (2003).

[8] D.C. Amberg, J.E. Zahner, J.W. Mulholland, J.R. Pringle, D. Botstein, Aip3p/Bud6p, a yeast actin-interacting protein that is involved in morphogenesis and the selection of bipolar budding sites, Mol. Biol. Cell 8 (1997) 729–753.

[9] K.R. Ayscough, J. Stryker, N. Pokala, M. Sanders, P. Crews, D.G. Drubin, High rates of actin filament turnover in budding yeast and roles for actin in establishment and maintenance of cell polarity revealed using the actin inhibitor latrunculin-A, J. Cell Biol. 137 (1997) 399–416.

[10] H. Jin, D.C. Amberg, Fission yeast Aip3p (spAip3p) is required for an alternative actin-directed polarity program, Mol. Biol. Cell 12 (2001) 1275–1291.

[11] N. Hachiya, R. Alam, Y. Sakasegawa, M. Sakaguchi, K. Mihara, T. Omura, A mitochondrial import factor purified from rat liver cytosol is an ATP- dependent conformational modulator for precursor proteins, EMBO J. 12 (1993) 1579–1586.

[12] N. Hachiya, T. Komiya, R. Alam, J. Iwahashi, M. Sakaguchi, T. Omura, K. Mihara, MSF, a novel cytoplasmic chaperone which functions in precursor targeting to mitochondria, EMBO J. 13 (1994) 5146–5154.

[13] N. Hachiya, K. Mihara, K. Suda, M. Horst, G. Schatz, T. Lithgow, Reconstitution of the initial steps of mitochondrial protein import, Nature 376 (1995) 705–709.

[14] A.E. Adams, J.R. Pringle, Relationship of actin and tubulin distribution to bud growth in wild-type and morphogenetic-mutant *Saccharomyces cerevisiae*, J. Cell Biol. 98 (1984) 934–945.

[15] P. Novick, D. Botstein, Phenotypic analysis of temperature-sensitive yeast actin mutants, Cell 40 (1985) 405–416.

[16] B. Schwikowski, P. Uetz, S. Fields, A network of protein–protein interactions in yeast, Nat. Biotechnol. 18 (2000) 1257–1261.

[17] T. Nishizaka, T. Yagi, Y. Tanaka, S. Ishiwata, Right-handed rotation of an actin filament in an in vitro motile system, Nature 361 (1993) 269–271.

Available online at www.sciencedirect.com
SCIENCE DIRECT®
Biochemical and Biophysical Research Communications 320 (2004) 1271–1276
BBRC
www.elsevier.com/locate/ybbrc

Oligomeric Aip2p/Dld2p forms a novel grapple-like structure and has an ATP-dependent F-actin conformation modifying activity in vitro

Naomi S. Hachiya,[a,b,c] Yuji Sakasegawa,[a,b] Hiroyuki Sasaki,[d] Akiko Jozuka,[a,b] Shoichiro Tsukita,[b,e] and Kiyotoshi Kaneko[a,c,*]

[a] *Department of Cortical Function Disorders, National Institute of Neuroscience, National Center of Neurology and Psychiatry, Tokyo 187-8502, Japan*
[b] *Tsukita Cell Axis Project, Exploratory Research for Advanced Technology (ERATO) and Solution Oriented Research for Science and Technology (SORST), Japan Science and Technology Corporation, Saitama 332-0012, Japan*
[c] *Core Research for Evolutional Science and Technology (CREST), Japan Science and Technology Agency, Saitama 332-0012, Japan*
[d] *Institute of DNA Medicine, The Jikei University School of Medicine, Tokyo 105-8461, Japan*
[e] *Department of Cell Biology, Faculty of Medicine, Kyoto University, Kyoto 606-8501, Japan*

Received 1 June 2004
Available online 26 June 2004

Abstract

In order to investigate the molecular mechanism of the F-actin conformation modifying activity [Biochem. Biophys. Res. Commun. 319 (2004) 78] of actin-interacting protein 2 (Aip2p) [Nat. Struct. Biol. 2 (1995) 28]/D-lactate dehydrogenase protein 2 (Dld2p) [Yeast 15 (1999) 1377; Biochem. Biophys. Res. Commun. 295 (2002) 910], the ultrastructure and the regulatory mechanism of the activity were further examined. Interestingly, a novel oligomeric grapple-like structure of 10–12 subunits with an ATP-dependent opening was observed. ATP regulates the opening and closing of the "gate" that forms the opening within oligomeric Aip2p/Dld2p, where binding to the substrate occurs while in the open form. In the presence of ATP (open state of oligomeric Aip2p/Dld2p), oligomeric Aip2p/Dld2p bound the F-actin fiber within the opening, whereas in the absence of ATP (closed state of oligomeric Aip2p/Dld2p), no binding was observed. Simultaneously, the oligomeric Aip2p/Dld2p increased the trypsin susceptibility of F-actin in an ATP-dependent manner. Use of the non-hydrolyzable ATP analogue AMP–PNP yielded similar results to those observed with ATP, suggesting that ATP binding rather than ATP hydrolysis is required for the protein conformation modifying reaction of oligomeric Aip2p/Dld2p. Endogenous Aip2p/Dld2p purified from *Saccharomyces cerevisiae* also exhibited such protein conformation modifying activity, but monomeric Aip2p/Dld2p with a C-terminal coiled-coil region-truncation failed to exhibit the activity. These data suggest that the oligomerization of Aip2p/Dld2p, which exhibits the unique grapple-like structure with an ATP-dependent opening, is required for the F-actin conformation modifying activity.

Keywords: Actin interacting protein 2; D-Lactate dehydrogenase protein 2; Oligomeric form; Grapple-like structure; F-actin; Trypsin susceptibility assay; ATP-dependent conformation modifying activity

Actin and its interacting proteins form an indispensable network in cells; a dynamic filament system that is crucial for endocytosis, exocytosis, locomotion, cell division, cytokinesis, shape, and various forms of intracellular motility. Among the actin-interacting proteins, the gene (YDL178w) encoding actin interacting protein 2 (Aip2p) was initially identified using a two-hybrid screen to search for *Saccharomyces cerevisiae* proteins that interact with actin [2]. Subsequently, the YDL178w gene product has been reported to localize on mitochondria and exhibit D-lactate dehydrogenase (DLD) activity in vitro, and therefore renamed as D-lactate dehydrogenase protein 2 (Dld2p) [3]. Besides, Schikowski et al. [5] suggested that the function of Aip2p may be associated with cell polarity by a computational analysis of protein–protein interactions in yeast. Thus, it was possible that Aip2p/Dld2p is multifunctional.

We previously reported that the Aip2p [2]/Dld2p [3,4] exhibits an interaction with F-actin both in vitro and in

* Corresponding author. Fax: +81-42-346-1748.
E-mail address: kaneko@ncnp.go.jp (K. Kaneko).

0006-291X/$ - see front matter © 2004 Elsevier Inc. All rights reserved.
doi:10.1016/j.bbrc.2004.06.082

vivo [1]. Incubation with Aip2p/Dld2p facilitated the formation of the circular form of F-actin in vitro, and the protease susceptibility of the Aip2p/Dld2p-bound "circular form" of F-actin increased, indicating that the Aip2p/Dld2p-bound "circular form" of F-actin possesses an aberrant conformation compared to the linear form of F-actin. When Aip2p/Dld2p was overexpressed in yeast cells, cells produced multibuds from the same mother neck or exhibited elongated bud necks, whereas AIP2-deleted cells displayed deformed morphology reflecting an inability to properly form the cleavage furrow during cell division, which was rescued by the introduction of wild-type Aip2p/Dld2p. While Aip2p/Dld2p-treated F-actin in the circular form was negligibly stained by rhodamine-labeled phalloidin (rhodamine–phalloidin) in vitro, rhodamine–phalloidin staining profiles in actin interacting protein 2 gene (AIP2)-modified cells suggested a correlation between the conformation of F-actin and the expression of Aip2p/Dld2p in vivo. Furthermore, the AIP2-deleted cells became sensitive to an osmotic condition, which is a hallmark of actin dysfunction, and Aip2p/Dld2p co-immunoprecipitated with actin in yeast cells. These properties suggest that Aip2p/Dld2p interacts with F-actin both in vitro and in vivo and plays an important role in the yeast cell morphology.

Under the background, here we further characterized the F-actin conformation modifying activity of Aip2p/Dld2p in terms of the ultrastructure and the regulatory mechanism of such activity. As results, we revealed that the activity requires a unique oligomeric grapple-like structure of 10–12 subunits with an ATP-dependent opening.

Materials and methods

Yeast strain and antibody. Wild-type yeast strains (ATCC24657) used in this study were purchased from American Type Culture Collection. Protease deficient strain SH2777 was a gift from Dr. Harashima, Osaka University. A synthetic peptide corresponding to the C-terminal 15 amino-acid residues of Aip2p/Dld2p (VHYDPNGILNPYKYI) was coupled through a COOH-terminal cysteine residue to BSA, and antibody was affinity purified using the antigen.

Trypsin susceptibility assay. The trypsin susceptibility assay was performed as previously described [1,6–8]. Briefly, assays (200 μl) were initiated by adding 200 ng of polymerized rabbit muscle actin to buffer A (10 mM Tris–Cl, pH 8.0, 0.1 M KCl, and 10 mM $MgCl_2$) containing 1 mM ATP and 500 ng of hexahistidine-tagged Aip2p/Dld2p, and incubated at 30 °C for 15 min. After incubation, samples were treated with trypsin (0.2 μg ml^{-1}) at 16 °C for 15 min. The reaction was terminated by incubation with soybean trypsin inhibitor (0.4 μg ml^{-1}) on ice for 5 min, TCA-precipitated with tRNA carrier, and then subjected to SDS–PAGE and Western blotting. To detect actin, affinity-purified polyclonal rabbit anti-actin antibody served as the primary antibody and horseradish peroxidase-linked IgG (ICN Pharmaceuticals) was the secondary antibody. Immunoreactive bands were visualized by ECL-plus (Amersham Biosciences) and analyzed using a Fluoro Smax (Bio-Rad).

Purification of hexahistidine-tagged Aip2p/Dld2p. In an effort to obtain sufficient quantities of Aip2p/Dld2p, the protein was prepared from the expression strain in yeast under control of the ADH promoter as previously described [1]. Briefly, the C-terminally hexahistidine-tagged YDL178w gene was amplified by PCR and inserted into the aureobasidin A (Ab A) selective expression vector pAUR123 (TaKaRa Biomedicals). The protease deficient strain SH2777 was transformed by this plasmid and transformants were grown on YPD plates containing 0.5 μg ml^{-1} Ab A. Inoculated medium (8 L) was incubated overnight at 30 °C to an OD at 600 nm of 1–2. Cells were collected, resuspended in four volumes of buffer B (50 mM NaPi, pH 8.0, 150 mM NaCl, and 10 mM imidazole), crushed using glass beads, and centrifuged at 10,000 rpm for 10 min at 4 °C. Supernatants were collected and ultracentrifuged at 100,000*g* at 4 °C for 1 h. The precipitate was resuspended, passed through a Ni–NTA agarose column (Qiagen, K.K.) equilibrated in buffer B, and subsequently eluted with buffer B containing 0.5 M imidazole. Eluted fractions were dialyzed against buffer C (10 mM Hepes–KOH, pH 7.4, 50 mM NaCl, and 1 mM DTT), applied to an ion exchange Mono Q column (Amersham–Pharmacia Biotech, AKTA System) equilibrated with buffer C, and eluted with a linear NaCl gradient (100–500 mM). Immunoreactive fractions were dialyzed against buffer D (50 mM NaPi, pH 7.5, 10 mM NaCl, and 1 mM Mg $(OAc)_2$), and finally passed through a Superdex 200 gel filtration column equilibrated with buffer D.

C-terminal coiled-coil domain-truncated Aip2p/Dld2p. To generate C-terminal coiled-coil domain-truncated Aip2p/Dld2p, the gene for the C-terminal 100 amino acid residue-truncated form of C-terminally hexahistidine-tagged Aip2p/Dld2p was amplified by PCR and inserted into the yeast expression vector pAUR123 (TaKaRa Biomedicals). The Aip2p/Dld2p-deleted strain was transformed by this plasmid, and transformants were checked by colony PCR, selected on YPD plates containing 500 ng ml^{-1} Ab A, inoculated, and the protein was finally purified.

Purification of endogenous Aip2p/Dld2p. Yeast microsome fraction from the yeast strain ATCC 24657 [MATα mal [rho+]CAN^S] (25 L) was incubated with buffer E (10 mM Hepes–KOH, pH 7.4, 1 mM DTT, and 1 mM $Mg(OAc)_2$) containing 500 mM NaCl on ice for 20 min and then centrifuged at 100,000*g* for 60 min at 4 °C. Following centrifugation, the salt-extracted fraction was dialyzed against buffer E overnight at 4 °C, passed through DEAE–Sepharose Fast Flow (Amersham Biosciences) equilibrated with buffer E, washed with 50 mM NaCl, and then eluted with 300 mM NaCl. The eluate was dialyzed against buffer E, passed through Resource Q (Amersham Biosciences), and eluted with a linear NaCl gradient (100–500 mM). Active fractions were further purified using hydroxyapatite (Seikagaku Kogyo) and ATP agarose (Sigma).

Results

In an effort to examine the structure of Aip2p/Dld2p by electron microscopy, we cloned the YDL178W gene and expressed it in yeast cells under control of the ADH promoter using an Ab A expression system (TAKARA, BIO) to yield highly purified protein [1]. Electron microscopic observation of purified Aip2p/Dld2p using rotary shadowing method [9] revealed that it possesses an unusual "grapple-like" oligomeric structure of ~10 nm in diameter within the opening (Fig. 1A, left panels). Furthermore, negative staining observation [10] revealed that oligomeric Aip2p/Dld2p adopted at least two different states that corresponded to an "open state" in the presence of ATP, or a "closed state" in the absence of ATP (Fig. 1A, right panels). Aip2p/Dld2p contains two ATP-binding Walker type B motifs